TABLE V. Correlation of Cardiac Measurements and Total Dose of THP

Measurements	Correlation coefficient	*P*
FS	0.01	0.09
EF	0.90	0.49
E/A ratio	0.08	0.57
CVNN	0.26	0.08
6MWT	0.02	0.88
BNP at rest	0.11	0.42
BNP after exercise	0.27	0.03

THP, pirarubicin; FS, fractional shortening; EF, ejection fraction. CVNN, co-variance of NN intervals; 6MWT, 6-min walk test.

was observed for subjects with $\geqq 300$ mg/m^2 of THP, but not for subjects with <300 mg/m^2 of THP. Although correlations between the measurements of left ventricular function (FS and EF) and cumulative THP dose or BNP levels were studied, no significant results were obtained (Supplemental Appendix).

DISCUSSION

THP is a derivative of DOX developed in Japan, and its cardiotoxicity may be lower than that of DOX [12–15]. Tsurumi et al. and Niitsu et al. reported that acute cardiotoxicity with THP was less frequent than that with DOX among adult lymphoma patients [17–20]. However, no studies for late cardiotoxicity of THP have been reported. In this study, cardiac function and biomarkers were measured in long-term survivors with ALL who received THP treatment and in whom no apparent cardiac dysfunction was detected. Thus, this is the first report of late cardiotoxicity of THP in cancer survivors.

The incidence of AC-induced cardiac dysfunction in childhood cancer survivors varied considerably across studies. The incidences of 14–24% for cardiac dysfunction assessed by echocardiography had been reported in five studies, in which median doses of cumulative AC ranged from 165 to 450 mg/m^2 [6,7,28,29,31]. Three other studies also reported that cumulative AC dose was significantly associated with reduced FS function, and high cumulative dose >300 mg/m^2 increased the risk of cardiac dysfunction [11,26,27]. When our results are compared with these findings, it appears that incidence of cardiac dysfunction after THP treatment

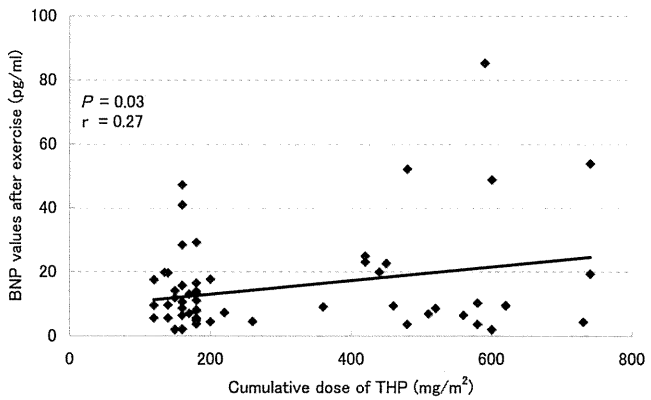

Fig. 1. Correlation between plasma BNP values after exercise and cumulative pirarubicin (THP) dose.

TABLE VI. Plasma BNP Levels According to Total Dose of THP

Total dose of THP	<300 mg/m^2 (n = 39)	$\geqq 300$ mg/m^2 (n = 21)	*P* value vs. <300 mg/m^2
BNP at rest (pg/ml)	12.5 ± 13.8	14.8 ± 15.8	0.56
BNP after exercise (pg/ml)	12.2 ± 9.9	20.6 ± 21.2	0.04
ΔBNP (pg/ml)	−0.3 ± 7.8	5.4 ± 8.1	0.01

Values are expressed as mean ± SD. THP, pirarubicin.

is relatively low. However, it should be noted that EF and FS may not be sensitive parameters for monitoring cardiac injury, because they often remain normal until critical point in the face of cardiac compensation [30]. Tissue Doppler echocardiography (TDE) has became widely available. Since TDE gives a more precise estimation for diastolic dysfunction than the E/A ratio used in this study, it may be helpful in future studies [40].

Non-invasive techniques for identifying patients who are at high-risk of developing AC-induced cardiomyopathy are critically important. For this purpose, natriuretic peptides including BNP and N-terminal fragment of BNP pro-hormone (NT-pro-BNP), are currently used for detection of cardiac injury in both adults and children [41]. Until now, 4 studies have reported BNP levels in childhood cancer survivors who received AC therapy [28–31]. In 3 of these, elevated BNP levels were detected [28,30,31], although the values did not significantly correlate with cumulative AC doses. Our study showed no significantly different BNP levels in patients from controls, but BNP levels after exercise were significantly correlated to cumulative THP dose. A similar finding was reported by Pinarli et al. [30], in which they found high BNP levels after exercise by treadmill, but no correlation with cumulative AC dose. Since augmented response in plasma BNP levels to exercise has been reported in adult patients with left ventricular dysfunction or exercise-induced ischemia [42,43], the increased BNP levels and ΔBNP after exercise in our study may be associated with subclinical myocardial injury. The stability of BNP in blood samples should be considered when interpreting BNP values after exercise. McNairy at al. found that post-exercise BNP returned to baseline levels within 60 min for normal subjects [44]. On the other hand, NT-pro-BNP is characterized by its stability against protease and longer half-life in comparison with BNP. Thus, the measurement of NT-pro-BNP may provide additional evidence in the early detection of anthracycline-induced cardiotoxicity in childhood and adolescence.

Currently, the 6MWT is considered to represent the most suitable method to assess the exercise tolerance. This self-paced test is easy to perform, well tolerated, and highly acceptable to children [39,45]. In our study, all subjects finished the test without difficulty or premature stopping. Consequently, the 6MWT may be used both in assessment and follow up of functional capacity in childhood cancer survivors.

In conclusion, the present study suggested that THP-induced late cardiac dysfunction is rare. However, further investigation is warranted to clarify the pathopsysiological significance of elevated BNP levels after the exercise test in asymptomatic patients.

ACKNOWLEDGMENT

We thank the patients who enrolled in this study and their families, and Paul Lewis for preparation of the manuscript.

REFERENCES

1. Hitchcock-Bryan S, Gelber R, Cassady JR, et al. The impact of induction anthracycline on long-term failure-free survival in childhood acute lymphoblastic leukemia. Med Pediatr Oncol 1986;14: 211–215.
2. Smith MA, Ungerleider RS, Horowitz ME, et al. Influence of doxorubicin dose intensity on response and outcome for patients with osteogenic sarcoma and Ewing's sarcoma. J Natl Cancer Inst 1991;83:1460–1470.
3. Giantris A, Abdurrahman L, Hinkle A, et al. Anthracycline-induced cardiotoxicity in children and young adults. Crit Rev Oncol Hematol 1998;27:53–68.
4. Scully RE, Lipshultz SE. Anthracycline cardiotoxicity in long-term survivors of childhood cancer. Cardiovasc Toxicol 2007;7: 122–128.
5. Beneficial and harmful effects of anthracyclines in the treatment of childhood acute lymphoblastic leukaemia: A systematic review and meta-analysis. Childhood Acute Lymphoblastic Leukaemia Collaborative Group (CALLCG). Br J Haematol 2009;145:376–388.
6. Lipshultz SE, Colan SD, Gelber RD, et al. Late cardiac effects of doxorubicin therapy for acute lymphoblastic leukemia in childhood. N Engl J Med 1991;324:808–815.
7. Steinherz LJ, Steinherz PG, Tan CT, et al. Cardiac toxicity 4–20 years after completing anthracycline therapy. JAMA 1991;266: 1672–1677.
8. Krischer JP, Epstein S, Cuthbertson DD, et al. Clinical cardiotoxicity following anthracycline treatment for childhood cancer: The Pediatric Oncology Group experience. J Clin Oncol 1997; 15:1544–1552.
9. Kremer LC, van Dalen EC, Offringa M, et al. Anthracycline-induced clinical heart failure in a cohort of 607 children: Long-term follow-up study. J Clin Oncol 2001;19:191–196.
10. Sorensen K, Levitt GA, Bull C, et al. Late anthracycline cardiotoxicity after childhood cancer: A prospective longitudinal study. Cancer 2003;97:1991–1998.
11. Lipshultz SE, Lipsitz SR, Sallan SE, et al. Chronic progressive cardiac dysfunction years after doxorubicin therapy for childhood acute lymphoblastic leukemia. J Clin Oncol 2005; 23:2629–2636.
12. Umezawa H, Takahashi Y, Kinoshita M, et al. Tetrahydropyranyl derivatives of daunomycin and adriamycin. J Antibiot 1979;32: 1082–1084.
13. Takagi T, Oguro M. (2-R)-4-o-Tetrahydropyranyladriamycin, a new anthracyclin derivative; its effectiveness in lymphoid malignancies. Cancer Chemother Pharmacol 1987;20:151–154.
14. Takagi T, Sakai C, Oguro M. Combination chemotherapy with pirarubicin (THP), cyclophosphamide, vincristine, and prednisolone (VEP-THP therapy) in the treatment of non-Hodgkins lymphoma. Oncology 1990;47:25–28.
15. Miller AA, Salewski E. Prospects for pirarubicin. Med Pediatr Oncol 1994;22:261–268.
16. Aoki S, Tsukada N, Nomoto N, et al. Effect of pirarubicin for elderly patients with malignant lymphoma. J Exp Clin Cancer Res 1998;17:465–470.
17. Niitsu N, Umeda M. Biweekly THP-COPBLM (pirarubicin, cyclophosphamide, vincristine, prednisone, bleomycin and procarbazine) regimen combined with granulocyte colony-stimulating factor (G-CSF) for intermediate- and high-grade non-Hodgkins's lymphoma. Leukemia 1998;12:1457–1460.
18. Niitsu N, Umeda M. Response and adverse drug reactions to combination chemotherapy in elderly patients with aggressive non-Hodgkin's lymphoma: Comparison of CHOP, COP-BLAM, COP-BLAM III, and THP-COPBLM. Eur J Haematol 1999;63: 337–344.
19. Tsurumi H, Yamada T, Sawada M, et al. Biweekly CHOP or THP-COP regimens in the treatment of newly diagnosed aggressive non-Hodgkin's lymphoma. A comparison of doxorubicin and pirarubicin: A randomized phase II study. J Cancer Res Clin Oncol 2004;130:107–113.
20. Zhai L, Guo C, Cao Y, et al. Long-term results of pirarubicin versus doxorubicin in combination chemotherapy for aggressive non-Hodgkin's lymphoma: Single center, 15-year experience. Int J Hematol 2010;91:78–86.
21. Kawa K, Ohnuma N, Kaneko M, et al. Long-term survivors of advanced neuroblastoma with MYCN amplification: A report of 19 patients surviving disease-free for more than 66 months. J Clin Oncol 1999;17:3216–3220.
22. Kaneko M, Tsuchida Y, Mugishima H, et al. Intensified chemotherapy increases the survival rates in patients with stage 4 neuroblastoma with MYCN amplification. J Pediatr Hematol Oncol 2002;24:613–621.
23. Tsurusawa M, Taga T, Horikoshi Y, et al. Favourable outcomes in children with diffuse large B-cell lymphoma treated by a short-term ALL-like regimen: A report on the NHL960 study from the Japanese Childhood Cancer and Leukemia Study Group. Leuk Lymphoma 2008;49:734–739.
24. Tsurusawa M, Shimomura Y, Asami K, et al. Long-term results of the Japanese Childhood Cancer and Leukemia Study Group studies 811, 841, 874 and 911 on childhood acute lymphoblastic leukemia. Leukemia 2010;24:335–344.
25. Yamaji K, Okamoto T, Yokota S, et al. Minimal Residual Disease-based Augmented Therapy in Childhood Acute Lymphoblastic Leukemia: A Report from The Japanese Childhood Cancer and Leukemia Study Group Study. Pediatr Blood Cancer 2010;55: 1287–1295.
26. Lipshultz SE, Lipsitz SR, Mone SM, et al. Female sex and drug dose as risk factors for late cardiotoxic effects of doxorubicin therapy for childhood cancer. N Engl J Med 1995;332:1738–1743.
27. Nysom K, Holm K, Lipsitz SR, et al. Relationship between cumulative anthracycline dose and late cardiotoxicity in childhood acute lymphoblastic leukemia. J Clin Oncol 1998; 16: 545–550.
28. Hayakawa H, Komada Y, Hirayama M, et al. Late cardiac evaluation of children with solid tumors after anthracycline chemotherapy. Med Pediatr Oncol 2001;37:4–9.
29. Poutanen T, Tikanoja T, Riikonen P, et al. Long-term prospective follow-up study of cardiac function after cardiotoxic therapy for malignancy in children. J Clin Oncol 2003;21:2349–2356.
30. Pinarli FG, Oguz A, Tunaoglu FS, et al. Late cardiac evaluation of children with solid tumors after anthracycline chemotherapy. Pediatr Blood Cancer 2005;44:370–377.
31. Aggarwal S, Pettersen MD, Bhambhani K, et al. B-Type natriuretic peptide as a marker for cardiac dysfunction in anthracycline-treated children. Pediatr Blood Cancer 2007;49:812–816.
32. The criteria committee of the New York Heart Association. Nomenclature and criteria for diagnosis of diseases of the heart and great vessels, 9th edition. Boston, MA: Little, Brown & Co; 1994.
33. Fletcher GF, Balady GJ, Amsterdam EA, et al. Exercise standards for testing and training: A statement for healthcare professionals from the American Heart Association. Circulation 2001;104: 1694–1740.
34. Shimosaka K, Takahashi A, Saitou H, et al. Evaluation of automated chemiluminescent immunoassay analyzer exclusive kit "MI02 Shionogi BNP". Igaku to Yakugaku 2005;53:353–360 (in Japanese).

35. Sahn DJ, DeMaria A, Kisslo J, et al. Recommendations regarding quantification in M-mode echocardiography: Result of a survey of echocardiographic measurements. Circulation 1978; 58:1072–1083.
36. Kimball TR, Michelfelder EC. Echocardiography, in Moss & Adams's "Heart Disease in Infants, Children, and Adolescents", 8th edition. Philadelphia: Lippincott Williams & Wilkins; 2008, pp. 95–162.
37. Bu'Lock FA, Mott MG, Oakhill A, et al. Left ventricular diastolic filling patterns associated with progressive anthracycline-induced myocardial damage: A prospective study. Pediatr Cardiol 1999;20:252–263.
38. Dorup I, Levitt G, Sullivan I, et al. Prospective longitudinal assessment of late anthracycline cardiotoxicity after childhood cancer: The role of diastolic function. Heart 2004;90:1214–1216.
39. Geiger R, Strasak A, Treml B, et al. Six-minute walk test in children and adolescents. J Pediatr 2007;150:395–399.
40. Civilibal M, Caliskan S, Oflaz H, et al. Left ventricular function by 'conventional' and 'tissue Doppler' echocardiography in paediatric dialysis patients. Nephrology (Carlton) 2009;14:636–642.
41. Mavinkurve-Groothuis AM, Kapusta L, Nir A, et al. The role of biomarkers in the early detection of anthracycline-induced cardiotoxicity in children: A review of the literature. Pediatr Hematol Oncol 2008;25:655–664.
42. Kato M, Kinugawa T, Ogino K, et al. Augmented response in plasma brain natriuretic peptide to dynamic exercise in patients with left ventricular dysfunction and congestive heart failure. J Intern Med 2000;248:309–315.
43. Foote RS, Pearlman JD, Siegel AH, et al. Detection of exercise-induced ischemia by changes in B-type natriuretic peptides. J Am Coll Cardiol 2004;44:1980–1987.
44. McNairy M, Gardetto N, Clopton P, et al. Stability of B-type natriuretic peptide levels during exercise in patients with congestive heart failure: Implications for outpatient monitoring with B-type natriuretic peptide. Am Heart J 2002;143:406–411.
45. Moalla W, Gauthier R, Maingourd Y, et al. Six-minute walking test to assess exercise tolerance and cardiorespiratory responses during training program in children with congenital heart disease. Int J Sports Med 2005;26:756–762.

Int J Hematol (2011) 93:135–137
DOI 10.1007/s12185-010-0754-y

LETTER TO THE EDITOR

Flow cytometric analysis of de novo acute myeloid leukemia in childhood: report from the Japanese Pediatric Leukemia/ Lymphoma Study Group

Hideaki Ohta · Shotaro Iwamoto · Nobutaka Kiyokawa · Masahito Tsurusawa · Takao Deguchi · Kozo Takase · Junichiro Fujimoto · Keizo Horibe · Yoshihiro Komada

Received: 6 August 2010 / Revised: 5 December 2010 / Accepted: 14 December 2010 / Published online: 5 January 2011

Immunophenotypic analysis has become a powerful tool for the correct identification of leukemic cell lineage. Our study evaluates the diagnostic utility of flow cytometric immunophenotyping of pediatric AML. We retrospectively collected data of immunophenotype from 375 cases of de novo AML studied from 1997 to 2007 at central laboratory institutions of the Japanese Pediatric Leukemia/Lymphoma Study Group (JPLSG): Department of Pediatrics and Developmental Science, Mie University Graduate School of Medicine; Department of Pediatrics, Osaka University Graduate School of Medicine; Center for Clinical Research, National Center for Child Health and Development; and Department of Pediatrics, Aichi Medical University. The diagnosis of AML was made according to the French-American-British (FAB) classification based on morphology and enzyme cytochemical analysis as follows: M0 (acute myeloid leukemia without differentiation, $n = 11$), M1 (acute myelocytic leukemia with little differentiation, $n = 41$), M2 (acute myelocytic leukemia with differentiation, $n = 113$), M4 (acute myelomonocytic leukemia, $n = 47$), M5 (acute monocytic leukemia, $n = 54$), M6 (acute erythroleukemia, $n = 6$), and M7 (acute megakaryoblastic leukemia, $n = 61$).

Mononuclear cells of bone marrow or peripheral blood samples were stained with various combinations of fluorescein isothiocyanate (FITC)- and phycoerythrin (PE)-labeled monoclonal antibodies against the following antigens: CD4, CD7, CD13, CD14, CD15, CD19, CD33, CD34, CD36, CD41, CD42b, CD45, CD56, CD61, CD65, CD117, glycophorin A (GPA: CD235a), and HLA-DR. Cytoplasmic MPO was also detected by anti-MPO antibody after permeabilization. Two-color flow cytometric immunophenotyping was performed by collecting 10,000 ungated list mode events. An antigen was considered as

For the Immunological Diagnosis Committee of the Japanese Pediatric Leukemia/Lymphoma Study Group.

H. Ohta (✉)
Department of Pediatrics,
Osaka University Graduate School of Medicine,
Yamadaoka 2-2, Suita, Osaka 565-0871, Japan
e-mail: ohta@ped.med.osaka-u.ac.jp

S. Iwamoto · T. Deguchi · Y. Komada
Department of Pediatrics and Developmental Science,
Mie University Graduate School of Medicine,
Tsu, Mie, Japan

N. Kiyokawa
Department of Developmental Biology,
National Center for Child Health and Development,
Setagaya-ku, Tokyo, Japan

M. Tsurusawa
Department of Pediatrics, Aichi Medical University,
Nagakute, Aichi, Japan

K. Takase
Department of Health Science Policies,
Division of Research Development,
Graduate School of Medical and Dental Sciences,
Tokyo Medical and Dental University,
Bunkyo-ku, Tokyo, Japan

J. Fujimoto
Center for Clinical Research, National Center for Child Health and Development, Setagaya-ku, Tokyo, Japan

K. Horibe
Clinical Research Center, National Hospital Organization
Nagoya Medical Center, Nagoya, Aichi, Japan

Table 1 Immunophenotypic profile of 375 de novo cases of acute myeloid leukemia

	CD34	CD117	HLADR	MPO	CD13	CD33	CD14	CD15	CD65	GPA	CD36	CD41	CD42b	CD61	CD7	CD4	CD19	CD56	CD45
M0 (11)	72.7 (11)	90.9 (11)	63.6 (11)	45.5 (11)	54.5 (11)	90.0 (11)	0 (11)	33.3 (9)	16.7 (6)	0 (11)	9.1 (11)	9.1 (11)	9.1 (11)	ND	54.5 (11)	9.1 (11)	9.1 (11)	45.5 (11)	90.0 (10)
M1 (41)	85.4 (41)	100 (36)	73.2 (41)	100 (41)	90.2 (41)	97.6 (41)	2.6 (39)	60.7 (28)	75.0 (20)	0 (37)	18.9 (37)	10.0 (40)	0 (36)	ND	51.2 (41)	2.7 (37)	7.3 (41)	19.5 (41)	90.9 (33)
M2 (113)	83.8 (111)	94.4 (89)	89.2 (111)	96.4 (84)	91.2 (113)	92.9 (113)	7.4 (108)	55.1 (89)	33.3 (63)	0 (93)	12.0 (92)	4.5 (112)	2.2 (92)	ND	14.3 (112)	0 (95)	24.8 (113)	36.4 (110)	97.3 (74)
M3 (42)	14.3 (42)	76.3 (38)	4.8 (42)	96.9 (32)	92.9 (42)	97.6 (42)	4.8 (42)	15.6 (32)	53.8 (26)	2.8 (36)	5.6 (36)	0 (42)	10.8 (37)	ND	0 (42)	2.7 (37)	2.4 (42)	7.1 (42)	85.2 (23)
M4 (47)	53.2 (47)	76.7 (43)	78.7 (47)	94.9 (39)	87.2 (47)	93.6 (47)	29.8 (47)	80.0 (30)	80.6 (31)	2.3 (43)	51.2 (43)	10.6 (47)	4.5 (44)	ND	8.5 (47)	23.1 (39)	2.1 (47)	15.2 (46)	94.4 (36)
M5 (54)	24.1 (54)	39.6 (48)	81.5 (54)	68.6 (35)	64.8 (54)	98.1 (54)	34.6 (52)	74.5 (47)	87.1 (31)	2.3 (43)	60.5 (43)	5.6 (54)	2.1 (48)	ND	3.7 (54)	52.1 (48)	1.9 (54)	57.4 (54)	93.8 (32)
M6 (6)	50.0 (6)	66.7 (6)	50.0 (6)	80.0 (5)	100 (6)	100 (6)	0 (6)	0 (4)	25.0 (4)	66.7 (6)	83.3 (6)	0 (6)	0 (6)	ND	33.3 (6)	16.7 (6)	0 (6)	0 (6)	60.0 (5)
M7 (61)	41.1 (56)	74.5 (51)	49.1 (57)	2.8 (36)	73.7 (57)	90.0 (60)	1.9 (53)	8.9 (45)	5.7 (35)	32.0 (50)	78.0 (50)	72.4 (58)	58.5 (53)	85.7 (14)	69.6 (56)	20.0 (50)	1.7 (58)	45.6 (57)	96.8 (31)

Values indicate proportion of positive cases (%); parentheses indicate evaluable cases, *ND* not done

positive, if more than 30% of the gated cells showed specific labeling above that of controls, or if positive subpopulation was distinctively identified even in <30% positive cases.

The result is summarized in Table 1. Cytoplasmic MPO expression was found in less than half of cases with M0 (45.5%), which is consistent with other reports [1, 2]. However, M0 blasts expressed CD33 (90.0%) and CD117 (90.9%), and, less frequently, CD34 (72.7%), suggesting myeloid lineage. The low expression of CD13 as compared to CD33 in our study may reflect a more mature myeloid profile in pediatric cases [1, 3]. CD7, expressed in more than half cases, is known to be expressed in a proportion of AML-M0 and M1 cases [3–5], consistent with the fact that CD7 is expressed during early stages of normal myeloid differentiation [6]. CD56 was also expressed in nearly half of cases, but only one case co-expressed CD7 and CD56 consistent with NK/myeloid-cell precursor acute leukemic cells [7].

M1 and M2 blasts expressed CD34, CD117, HLA-DR, MPO, CD13, CD33, and HLA-DR in more than 80% of cases, and less commonly CD15 and CD65. CD7 was detected in 51.2% of M1 cases, while its expression was repressed in M2. CD19, detected in 24.8% of M2 cases, was reported to be detected in 78–81% of M2 cases with t(8;21) translocation [8, 9].

M3 cells expressed CD13, CD33, and MPO at high frequency, as for M1 or M2 cells. However, the frequency of CD117 expression was 76.7%, lower than for M1 or M2 cells. A striking feature is that the expression of CD34 and HLA-DR was low, at 14.3 and 4.8%, respectively. The lack of CD34 and HLA-DR was a feature of M3 blasts [4, 5, 10].

Leukemic cells of most M4 and M5 cases expressed monocyte markers, CD15 and CD65. The less common expression of CD14 has been reported by others, particularly in M5 cases [2, 5, 10]. M4 and M5 expressed CD33 at similarly high frequencies. The progenitor-associated antigens, CD34 and CD117, were seen in a lower proportion of M5 cases, which might reflect commitment to monocytic lineage. CD4 was expressed in 52.1% of M5 cases and 23.1% of M4 cases, in line with other reports [2, 10].

We observed only six M6 cases. Leukemic erythroblasts expressed CD36 and GPA in 66.7 and 83.3% of cases, respectively. Myeloid antigens (MPO, CD13, and CD33) and hematopoietic progenitor-associated markers (CD34 and CD117) were also expressed at variable frequencies. The expression of monocytic markers (CD14 and CD15) was absent, as well as megakaryocyte-associated antigens (CD41 and CD42b).

The expression frequencies of megakaryocyte-associated antigens, CD41 and CD42b in cases with M7, were

72.4 and 58.5%, respectively. All cases expressed CD41 and/or CD42b. CD36 was expressed at a high frequency, but its expression was also seen in other subtypes (M4, M5, and M6). Myeloid antigens (CD13 and CD33) were expressed in most cases, but lack of MPO expression was observed. Hematopoietic progenitor-associated antigens (CD34 and CD117) were expressed in many cases, and CD7 was expressed in 69.6% of cases.

In conclusion, each subtype of AML possesses distinguishing features of antigen expression. Some antigens appear to be associated with certain subtypes, but are not necessarily specific. Uncommon expression must be interpreted in the context of the entire immunophenotyping profile for correct identification of AML subtypes.

Acknowledgment This study was supported by a grant for Clinical Cancer Research from the Ministry of Health, Labour, and Welfare of Japan.

References

1. Bene MC, Bernier M, Casasnovas RO, Castoldi G, Doekharan D, van der Holt B, et al. Acute myeloid leukaemia M0: haematological, immunophenotypic and cytogenetic characteristics and their prognostic significance: an analysis in 241 patients. Br J Haematol. 2001;113:737–45.
2. Behm FG. Diagnosis of childhood acute myeloid leukemia. Clin Lab Med. 1999;19:187–237. vii.
3. Kotylo PK, Seo IS, Smith FO, Heerema NA, Fineberg NS, Miller K, et al. Flow cytometric immunophenotypic characterization of pediatric and adult minimally differentiated acute myeloid leukemia (AML-M0). Am J Clin Pathol. 2000;113:193–200.
4. Creutzig U, Harbott J, Sperling C, Ritter J, Zimmermann M, Loffler H, et al. Clinical significance of surface antigen expression in children with acute myeloid leukemia: results of study AML-BFM-87. Blood. 1995;86:3097–108.
5. Kaleem Z, Crawford E, Pathan MH, Jasper L, Covinsky MA, Johnson LR, et al. Flow cytometric analysis of acute leukemias. Diagnostic utility and critical analysis of data. Arch Pathol Lab Med. 2003;127:42–8.
6. Chabannon C, Wood P, Torok-Storb B. Expression of CD7 on normal human myeloid progenitors. J Immunol. 1992; 149:2110–3.
7. Oshimi K. Progress in understanding and managing natural killer-cell malignancies. Br J Haematol. 2007;139:532–44.
8. Kita K, Nakase K, Miwa H, Masuya M, Nishii K, Morita N, et al. Phenotypical characteristics of acute myelocytic leukemia associated with the t(8;21)(q22;q22) chromosomal abnormality: frequent expression of immature B-cell antigen CD19 together with stem cell antigen CD34. Blood. 1992;80:470–7.
9. Hurwitz CA, Raimondi SC, Head D, Krance R, Mirro J Jr, Kalwinsky DK, et al. Distinctive immunophenotypic features of t(8;21)(q22;q22) acute myeloblastic leukemia in children. Blood. 1992;80:3182–8.
10. Campana D, Behm FG. Immunophenotyping of leukemia. J Immunol Methods. 2000;243:59–75.

Biochemical and Biophysical Research Communications 417 (2012) 162–168

Contents lists available at SciVerse ScienceDirect

Biochemical and Biophysical Research Communications

journal homepage: www.elsevier.com/locate/ybbrc

Transducible form of p47^{phox} and p67^{phox} compensate for defective NADPH oxidase activity in neutrophils of patients with chronic granulomatous disease

Fumiko Honda [a], Yumiko Hane [a], Tomoko Toma [b], Akihiro Yachie [b], Eun-Sung Kim [c], Sang-Kyou Lee [c], Masatoshi Takagi [a], Shuki Mizutani [a], Tomohiro Morio [a,*]

[a] Department of Pediatrics and Developmental Biology, Tokyo Medical and Dental University Graduate School of Medical and Dental Sciences, Tokyo, Japan
[b] Department of Pediatrics, Kanazawa University School of Medicine, Kanazawa, Japan
[c] Department of Biotechnology, Yonsei University, Seoul, Republic of Korea

ARTICLE INFO

Article history:
Received 8 November 2011
Available online 25 November 2011

Keywords:
Protein transduction
Chronic granulomatous disease (CGD)
NADPH oxidase
Reactive oxygen species (ROS)
Primary immunodeficiency

ABSTRACT

Protein delivery to primary cells by protein transduction domain (PTD) serves as a novel measure for manipulation of the cells for biological study and for the treatment of various human conditions. Although the method has been employed to modulate cellular function *in vitro*, only limited reports are available on its application in the replacement of deficient signaling molecules into primary cells. We examined the potential of recombinant proteins to compensate for defective cytosolic components of the NADPH oxidase complex in chronic granulomatous disease (CGD) neutrophils in both p47^{phox} and p67^{phox} deficiency. The p47^{phox} or p67^{phox} protein linked to Hph-1 PTD was effectively expressed in soluble form and transduced into human neutrophils efficiently without eliciting unwanted signal transduction or apoptosis. The delivered protein was stable for more than 24 h, expressed in the cytoplasm, translocated to the membrane fraction upon activation, and, most importantly able to restored reactive oxygen species (ROS) production. Although research on human primary neutrophils using the protein delivery system is still limited, our data show that the protein transduction approach for neutrophils may be applicable to the control of local infections in CGD patients by direct delivery of the protein product.

1. Introduction

Chronic granulomatous disease (CGD) is a primary immunodeficiency that affects phagocytes of the innate immune system and is characterized by recurrent life-threatening bacterial and fungal infections. The disease is caused by the lack of a component of NADPH oxidase complex [1]. NADPH oxidase is a multicomponent enzyme that is critical in non-mitochondrial ROS production, and is composed of a flavocytochrome b558 (gp91^{phox} and p22^{phox}), cytosolic components (p40^{phox}, p47^{phox}, and p67^{phox}) and a small GTP-binding protein (Rac1 or Rac2) [2]. About 60% of CGD cases are caused by mutations in the gene encoding gp91^{phox} located on X chromosome. Mutation in *NCF1* (encoding p47^{phox}) causes the most common autosomal recessive form of CGD accounting for approximately 20% of all CGD cases. Mutation in *NCF2* (encoding p67^{phox}) accounts for about 5% of all CGD cases [1,3]. Hematopoietic cell transplantation is currently the only proven curative therapy, but is often associated with transplant-related mortality [1,4]. There has been no effective therapeutic method to modulate neutrophil function or to reconstitute the functional defects in CGD neutrophils.

The intracellular delivery of proteins or peptides, has been difficult to achieve until recently, primarily due to plasma membrane barrier restrictions on the uptake of macromolecules. Cell penetrating peptide or protein transduction domain (PTD) is a short peptide of generally fewer than 30 amino acids that can cross biological membranes in a receptor- and cell-cycle-independent manner [5–7]. PTD is especially useful for delivery of large molecules into transfection-resistant cells, and can be incorporated into virtually any types of cells [5,8,9].

The protein transduction technique has most commonly been employed for modulation of specific protein–protein interactions with target transcription factors, signal transduction proteins, and cell cycle mediators [10]. Specific proteins and peptides for therapeutic targeting of oncogenes have been developed and tested *in vitro* and with *in vivo* animal models [10,11]. The protein transduction approach has also been used for delivery of active enzymes or other functional molecules in neurodegenerative disorders and metabolic diseases. PTD enzyme replacement *in vitro* has been successfully demonstrated in many previous publications [12–14]; however, their potential advantage as a method for intracellular replacement therapy *in vivo* is still largely unknown.

* Corresponding author. Address: Department of Pediatrics and Developmental Biology, Tokyo Medical and Dental University Graduate School of Medical and Dental Sciences, 1-5-45 Yushima, Bunkyo-Ku, Tokyo 113-8519, Japan. Fax: +81 3 5803 5245.
E-mail address: tmorio.ped@tmd.ac.jp (T. Morio).

0006-291X/$ - see front matter © 2011 Elsevier Inc. All rights reserved.
doi:10.1016/j.bbrc.2011.11.077

Replacement of functional signaling molecules by PTD techniques in cells is more technically demanding than delivery of protein–protein interaction modulators or active enzymes. This is because, in PTD, the delivered protein should be expressed at a physiological level, targeted to the specific cellular location, associated with other molecules, modified and translocated upon stimulation, and biologically active as long as the endogenous molecule.

The objective of this study was to compensate neutrophil dysfunction in CGD lacking a cytosolic component of the NADPH oxidase complex by the protein delivery system using Hph-1, an 11-amino acid long unique peptide of human origin, as PTD [15,16]. To achieve this, the transduced protein should function as its endogenous counterpart inside the cells. Activation of the complex is tightly controlled by plasma membrane targeting and/or phosphorylation of the cytosolic components [2,17]. Upon priming signal that activates PI3K, Rac2 released from GDP-dissociation inhibitor translocates to the membrane. During activation, p47 is phosphorylated on multiple Serines by PKC, leading to the translocation of the p47/p67/(p40) complex to the membrane [2,17,18]. The cytosolic components should locate in the cytoplasm in resting state, receive modification upon activation, associate with other molecules, and translocate to the membrane.

We also investigated possibility of the protein transduction to activate, or induce apoptosis in, neutrophils. Neutrophils have a short lifespan in the periphery and *ex vivo*, and the cells are quickly responsive and sensitive to the external stimuli, all factors that render cell manipulation even more difficult. Neutrophils sense microbes through various receptors, engulf foreign bodies, and are destined to undergo apoptosis after production of reactive oxygen species (ROS) and releasing neutrophil extracellular traps [19,20]. It has been postulated that PTD-mediated delivery of macromolecules does not elicit the innate immune response or cytotoxicity [9,10,13], but, to our knowledge, the cellular reactions elicited by protein delivery has not been formally addressed in human neutrophils.

We show here evidence that PTD-based protein delivery does not elicit non-specific activation or apoptosis of human neutrophils. We show that transduced recombinant p47 or p67 protein linked to Hph-1 distributes to a physiological location (i.e., moving to the plasma membrane) and restores normal ROS production in CGD neutrophils deficient in p47 or p67, respectively.

2. Results

2.1. Transduction efficacy of recombinant protein into human neutrophils and its effect on neutrophil activation and apoptosis

We first generated a construct for Hph-1-EGFP as a control protein for assessing expression kinetics, activation, and cellular apoptosis in neutrophils following protein transduction (Fig. 2A). The EGFP recombinant was expressed in bacteria, purified, treated with polymyxin B, and incubated with 1×10^6 purified human neutrophils with various concentrations and for various time periods. The recombinant was similarly incubated with human activated T-cells (CD3+ ≥95%) and with human B-cell line (i.e., Daudi cells).

The kinetics study monitored by flow cytometer showed the expression level at 10 min was higher in neutrophils compared to that in activated T-cells and Daudi cells. In neutrophils, the expression level reached a maximum by 30 min; and ⩾95% of the recombinant protein was expressed, while in activated T-cells the level peaked at 60 min (Fig. 3A).

The transduced protein was easily detectable in the cytoplasm at 1 μM by confocal fluorescence microscopy (CFM) as well as by flow cytometer, and the expression was increased in a dose dependent fashion (Fig. 3B and C). The dose–response was similar to that in Daudi cells; but significantly more EGFP protein was detected in neutrophils than in activated T-cells. The expression was detected at least up until 24 h post-Hph-1-EGFP transduction, suggesting that no major biodegradation of incorporated protein occurred (Fig. 3D).

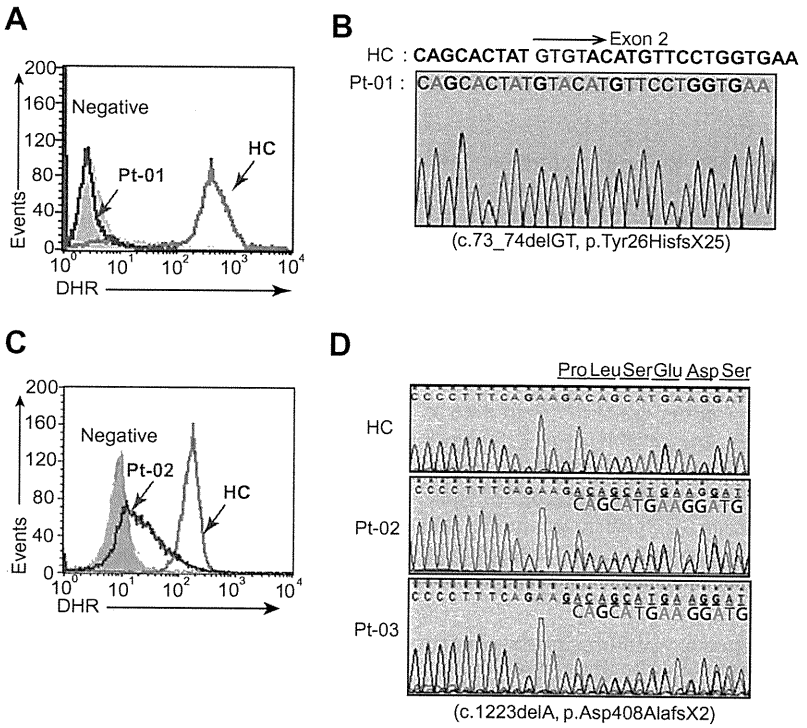

Fig. 1. Diagnosis of CGD in patients 1, 2, and 3 by assessment of ROS production and by sequencing analysis. (A and C) A representative FACS histogram for assessment of ROS production, measured by DHR123 fluorescence in purified neutrophils from healthy control (HC), p47-deficiency patient (Pt-01) (A) and from p67 deficiency (Pt-02) (C). (B and D) A result of sequencing analysis of *NCF1* in Pt-01 (B) and *NCF2* in Pt-02 and Pt-03 (D).

A

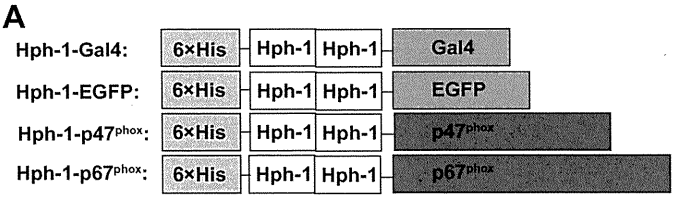

B

Primer	Sequence	Restriction enzyme
Gal4	5'-*GAATTC*AAGCTACTGTCTTCTATC-3'	*EcoR I*
	5'-*AAGCTT*CGGCGATACAGTCAA-3'	*Hind III*
EGFP	5'-*GAATTC*GTGAGCAAGGGCGAGGAG-3'	*EcoR I*
	5'-*AAGCTTT*CCTTGTACAGCTCGTCCATG-3'	*Hind III*
$p47^{phox}$	5'-*GAATTC*GGGGACACCTTCATCCGTC-3'	*EcoR I*
	5'-*AAGCTT*GACGGCAGACGCCAGCTTCCGC-3'	*Hind III*
$p67^{phox}$	5'-*GAATTC*TCCCTGGTGGAGGCCATCAGCCT-3'	*EcoR I*
	5'-*AAGCTTC*TAGACTTCTCTCCGAGTGCTTTCT-3'	*Hind III*

Fig. 2. Schematic diagram of Hph-1-recombinant constructs. (A) Schematic diagram of Hph-1-Gal4, Hph-1-EGFP, Hph-1-$p47^{phox}$, and Hph-1-$p67^{phox}$. (B) Primer sequences for construction of the indicated Hph-1-recombinant protein.

We next examined whether the transduction of foreign protein *per se* activates neutrophils or potentially elicits cellular damage leading to augmented or earlier apoptosis. Fig. 3D shows that the proportion of apoptotic cells does not increase in neutrophils transduced with Hph-1-EGFP compared to untreated neutrophils. Induction of Hph-1-EGFP did not induce significant activation of tyrosine kinases, activation of Akt, or phosphorylation of the intracellular components of the NADPH oxidase complex (Fig. 3E). Similarly, ROS production was not observed upon transduction with Hph-1-EGFP protein in addition to fMLP in control neutrophils. The similar results were obtained when neutrophils were treated with Hph-1-Gal4 (data not shown).

2.2. Hph-1-$p47^{phox}$ and Hph-1-$p67^{phox}$ compensate for defective NADPH oxidase activity in neutrophils of autosomal recessive CGD patients

We hypothesized that restoring intracellular p47 or p67 by protein delivery would correct defective NADPH activity, if the transduced protein were functional. To test this, we designed constructs

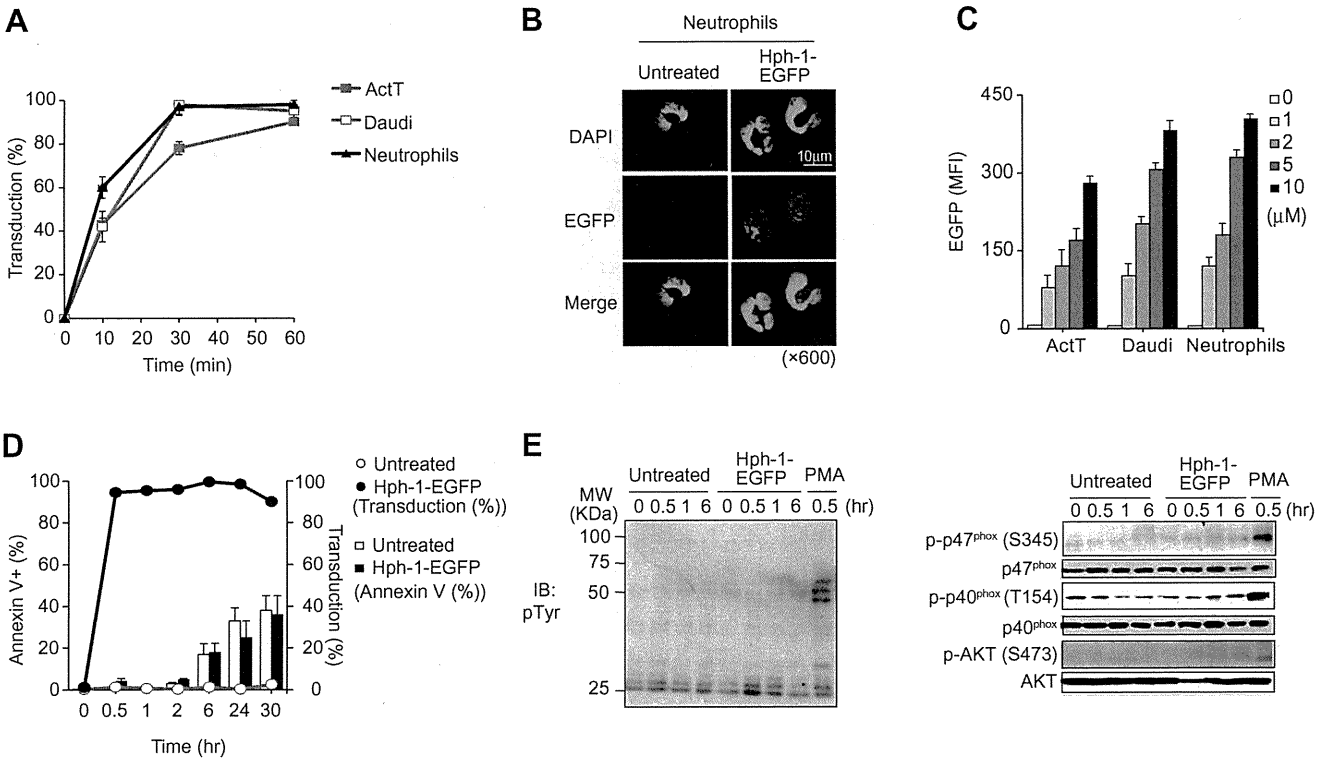

Fig. 3. Time-dependent and concentration-dependent transduction of Hph-1-EGFP in human neutrophils, and the effect of transduction on cellular activation and apoptosis. (A) Time dependent transduction kinetics of Hph-1-EGFP in human neutrophils, activated T-cells (ActT), and Daudi cells. (B) CFM analysis of transduced protein. (C) Concentration dependent intracellular delivery of EGFP in human neutrophils, activated T-cells (ActT), and Daudi cells ($n = 3$). (D) Percentage of neutrophil apoptosis and EGFP-positivity after EGFP protein delivery. Summary of three independent experiments is shown. (E) Tyrosine phosphorylation of neutrophil proteins, activation of AKT, or phosphorylation of cytosolic factors of NADPH oxidase complex after transduction of Hph-1-EGFP. One representative Western blot out of three independent experiments is shown. Mean + SD is indicated in (A, C, and D).

for Hph-1-p47^{phox} and Hph-1-p67^{phox} (Fig. 2A) and investigated their capacity to confer the ability to produce ROS in CGD neutrophils either lacking in p47 or p67. Hph-1-p47^{phox} and Hph-1-p67^{phox} were expressed abundantly and recovered insoluble fraction in BL21DE3 *Escherichia coli* strain at 37 °C incubation (Fig. 4A).

To determine the efficacy of transduction, the p47 protein was incubated with 10^6 purified neutrophils from p47-deficiency at various concentrations, and their expression was checked by Western blotting (Fig. 4B). The expression level of p47 was equivalent to that in control neutrophils when incubated at 1–5 μM for 30 min.

To confirm that Hph-1 induced p47 into the cells, we carried out CFM and Western blotting. CFM visualized the presence of p47 in the cytoplasm prior to stimulation, and the colocalization of p47 and gp91 at the membrane after PMA treatment in >95% of the cells (Fig. 4C). We also prepared cytoplasmic and membrane fractions from Hph-1-p47^{phox} transduced neutrophils and carried out anti-p47 Western blotting. The analysis further confirmed that the incorporated p47 protein, and endogenous p67, were located in the cytoplasm, but not in the membrane (Fig. 4C).

We then asked whether the transduced Hph-1-p47^{phox} was functional by measuring PMA-induced ROS production in the neutrophils from Pt-01. The Hph-1-p47^{phox} delivery restored the capacity to generate ROS in p47-deficient CGD neutrophils, while the additional expression did not result in augmented ROS release in control neutrophils (Fig. 4D). Transduction of the p47 recombinant did not enhance apoptosis as examined by Annexin V staining until 24 h post protein delivery (Fig. 4E). The delivery did not induce cellular activation in neutrophils detected by anti-phosphotyrosine blot (Fig. 4F). In addition, the transduced p47 was still detectable at 24 h as observed in Hph-1-EGFP transduction.

Five-times more expression of p67 was observed in p67-deficient neutrophils compared to control neutrophils when Hph-1-p67^{phox} was incubated at 5 μM for 30 min (Fig. 4G). The p67 expression was observed in >90% of the transduced cells by enumeration under CFM. DHR123 assay and luminol assay demonstrated that the intracellular delivery of p67 protein via Hph-1 restored the capacity to generate ROS in response to PMA in p67-deficient CGD neutrophils (Fig. 4H and I). ROS production in the transduced cells was slightly reduced compared to normal neutrophils, when the expression level of the recombinant was adjusted to the level of endogenous p67 (by incubation at 1 μM), but the difference was not statistically significant (Fig. 4H and I). Neither apoptosis nor ROS production was observed in control neutrophils transduced with Hph-1-p67^{phox}.

3. Discussion

In this paper, we have demonstrated that Hph-1-based protein delivery restores neutrophil ROS production in p47^{phox}-deficient and p67^{phox}-deficient CGD patients. The Hph-1-p47^{phox} and Hph-1-p67^{phox} was recovered in soluble fraction in large quantity in bacteria, and the transduction efficacy to neutrophils was at least more than 80%. The transported protein was localized in the cytosol of neutrophils and was translocated, upon stimulation, to the membrane associating with flavocytochrome b558 to cause the activation of NADPH oxidase. The cellular concentration of the recombinant was observed in a concentration-dependent manner, and thus was adjustable to the target level of choice. The PTD-mediated protein delivery *per se* did not trigger neutrophil activation or affect neutrophil cell survival.

To date, many groups in wide arenas of clinical and basic biology are working toward PTD-based delivery of therapeutic molecules. The diseases being treated *in vitro* or *in vivo* animal systems range from cancer, ischemia, neurodegenerative disease, and enzyme deficiency [8,11,14]. Despite the notable successes and high expectations, the use of PTD to deliver proteins has yet to become common place in cell biology, especially in fields using primary cells. This can be ascribed to inefficient protein expression, insolubility of protein, and biodegradation in transduced cells. In particular, research on primary neutrophils using protein delivery system has been limited; and most of the existing research employed peptide fragments for functional modulation of neutrophils [21,22].

Correction of defective molecule in neutrophils has not yet been attempted with PTD-based approach, much less for the replacement of cytoplasmic protein defective in CGD phagocytes. A pioneering work by Polack et al. has shown that the *Pseudomonas aeruginosa* strain harboring a plasmid encoding ExoS-N-terminal p67 fusion protein, CHA-pBP31, can infect an EBV-transformed cell line from p67-deficient CGD [23]. CHA-pBP31 was able to reconstitute the NADPH oxidase activity, to approximately 40% of normal at MOIs of 5 or 10. The system, however, is labor-intensive, has limits in deliverable molecular size, and is toxic at higher MOI. However, the intracellular delivery of p67 protein can now be achieved more easily, safely, effectively, and in more controlled manner with our PTD-based system.

The only curative therapies available for CGD are hematopoietic cell transplantation and gene therapy, both of which are associated with therapy-related toxicity and adverse effects [1,4]. In addition, infection control is critically important for the success of these curative therapies [1,4]. The true potential of the Hph-1-p47^{phox} and Hph-1-p67^{phox} as a therapeutic measure to correct deficient ROS production is yet to be tested in animal models. This protein delivery can be used, however, in local control of infection of the CGD patients, for example, by using as an ointment, or by applying the protein directly to the site of infection.

PTD-based enzyme replacement therapy has been proven effective in only limited cases or primary immunodeficiency. Purine nucleotide phosphorylase (PNP) is an intracellular enzyme critical for purine degradation, and PNP defects result in severe T-cell immunodeficiency. One study has reported that PNP fused to TAT rapidly enters PNP-deficient lymphocytes and increases intracellular enzyme activity for 96 h [12]. The same group has demonstrated in PNP$^{-/-}$ mice that TAT induced rapid and efficient delivery of active PNP into many tissues, including the brain, leading to correction of metabolic diseases and immune defects [13].

The protein transduction system thus can be applied for the correction of other immuno deficiencies lacking the intracellular enzyme or cytoplasmic signal molecule, either in part or entirely. The examples include severe congenital neutropenia due to mutation in *HAX1*, *ELA2*, or *MPO* and severe combined immunodeficiency caused by mutation in *JAK3*, *LCK*, *DCLRE1C*, *NHEJ1*, and *LIGIV*. Although the efficacy and safety should be examined in detail with an *in vivo* animal model system, clinical applications of these approaches would become a useful therapeutic option, until the time the patients receive curative therapy (e.g., hematopoietic cell transplantation or gene therapy). The unique ability of PTD will facilitate the design of therapeutic proteins that are defective in primary immunodeficiency.

4. Materials and methods

4.1. Case presentation

Pt-01 is 31-year-old female with recurrent skin infection, otitis, and genital candidiasis. She developed CGD colitis at the age of 19. PMA-driven ROS production of neutrophils as assessed by DHR123 staining is minimal (Fig. 1A). Sequencing analysis of the four NADPH oxidase genes (*CYBA*, *CYBB*, *NCF1*, and *NCF2*) revealed the homozygous c.73_74delGT mutation in *NCF1* (Fig. 1B).

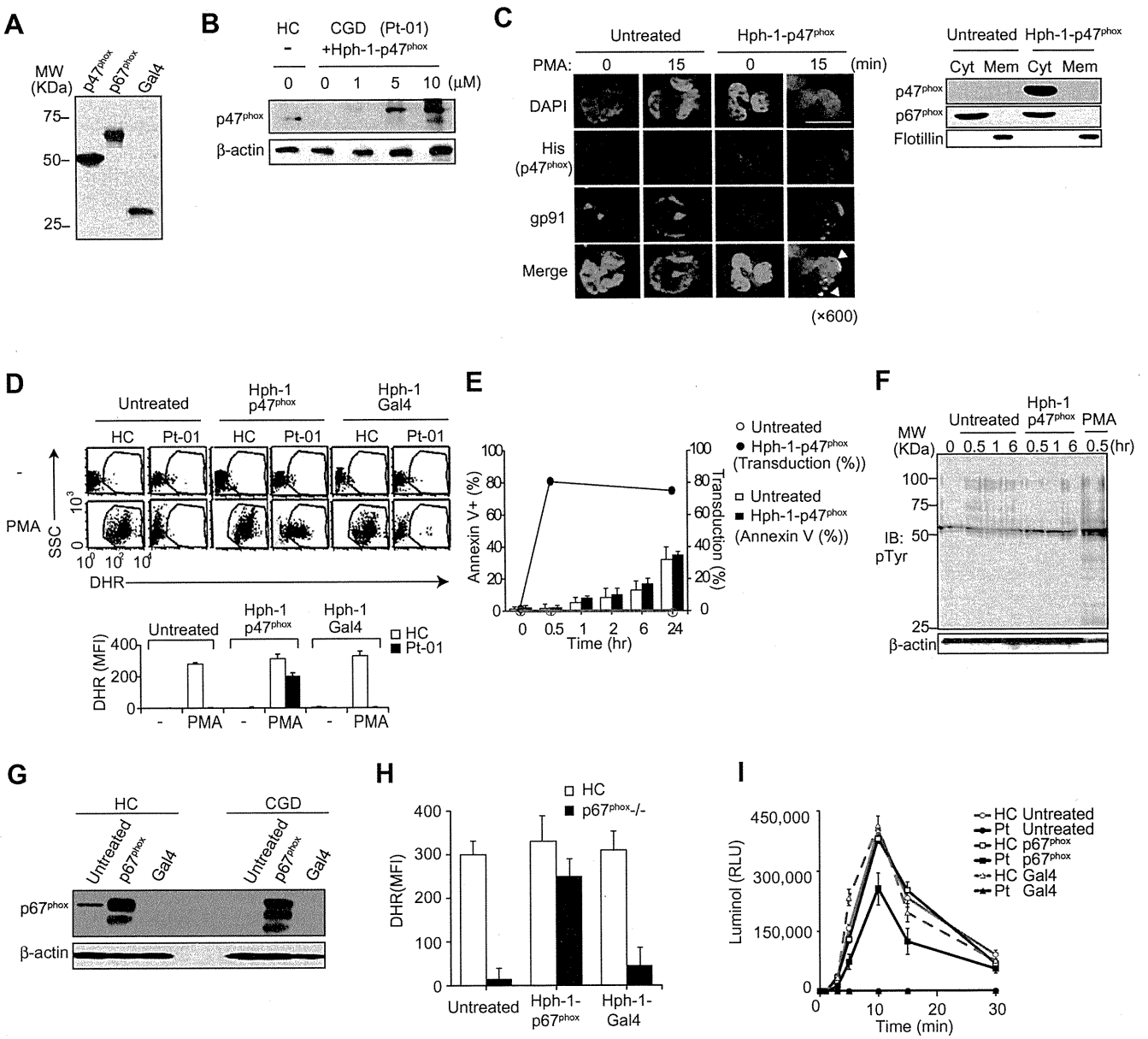

Fig. 4. The delivery of a cytosolic factor of NADPH oxidase complex via Hph-1 PTD results in the expression in the cytoplasm, co-localization with gp91 in the membrane upon stimulation, and restored ROS production in neutrophils from p47- and p67-deficiency. (A) Coomassie Brilliant Blue staining of the purified Hph-1-p47^{phox}, -p67^{phox}, and -Gal4 protein. (B) Expression of p47 in control neutrophils and in p47 deficiency transduced with indicated concentration of Hph-1-p47^{phox}. A representative data out of three independent experiments is shown. Actin is shown as a loading control. (C). Intracellular localization of transduced p47 assessed by CFM (left panel) and by WB (right panel). Flotillin was used as a membrane marker. (D) ROS production assessed by DHR123 staining in control neutrophils and in p47-deficient neutrophils that were transduced with Hph-1-p47^{phox} or with Hph-1-Gal4, and were stimulated as indicated. DMSO was used as a control reagent. Summary of three independent experiments is shown in the lower panel. (E) Percentage of apoptotic cells and p47-expressing cells in p47-negative CGD neutrophils incubated with or without Hph-1-p47^{phox}. Apoptosis was assessed by Annexin V staining, and percentage of p47-positive cells was enumerated by counting the cells with cytoplasmic p47 expression under CFM. (F) Anti-phosphotyrosine blot following transduction of Hph-1-p47^{phox} in p47-deficient neutrophils. (G) Expression of p67 in neutrophils from HC and from p67-deficiency with or without transduction of indicated recombinant protein. One representative data out of three independent experiments for Pt-02 and Pt-03 is shown. (H) Mean DHR123 fluorescence in control neutrophils and in p67-deficient neutrophils, transduced with or without the indicated recombinant. Combined results from three independent experiments for Pt-02 and Pt-03 are shown. (I) Time course of PMA-driven H_2O_2 production, measured by a luminol assay, in control neutrophils and p67-deficiency neutrophils with or without Hph-1-p67^{phox} transduction. One representative data is shown. The experiment was repeated three times in three HCs and p67 deficient patient (Pt-02). HC: healthy control. Mean + SD is shown in D, E, H, and I.

Pt-02 is 8-year-old boy who developed perianal abscess and cervical lymphoadenopathy at 1-year old. Bacterial culture of the abscess revealed the presence of *Serratia marcescens* and Group A *Streptococci*. The DHR123 assay revealed positive but significantly attenuated ROS production (Fig. 1C). Sequencing of the four NADPH oxidase genes revealed a homozygous c1233delA mutation in *NCF2* (Fig. 1D).

Pt-03 is currently 2-year-old girl and is a younger sister of Pt-02. The patient harbored the same mutation in *NCF2* detected in Pt-02. Pt-03 was well until 2-months old when she developed diarrhea of unknown origin lasting for >8 weeks. Pt-02 and Pt-03 have been on Sulfamethoxazole-Trimethoprim and Itraconazole after diagnosis of CGD and have been well without major infection. However, perianal abscess frequently recurs in Pt-02.

Written informed consent was obtained from all subjects (or their parents). The study protocol was approved by the ethics committee of the Faculty of Medicine, Tokyo Medical and Dental University.

4.2. Reagents

Anti-phosphotyrosine mAb (4G10) and rabbit polyclonal antibody to gp91^{phox} were from Upstate. Mouse mAb to flotillin-1, p67^{phox}, and isotype-matched FITC-mouse IgG were from BD Pharmingen. Mouse mAbs to phospho-AKT, to p47^{phox} were from Rockland Immunochemicals, and from Santa-Cruz, respectively. MAbs to 6x His and to phospho-p40^{phox} were obtained from Cell signaling technology. Antibody directed against phosphor-Ser345 was generated in rabbits by injection with ovalbumin conjugated to the phosphopeptide sequence of p47^{phox} (QARPGPQS [phospho]PGSPLEEE). PMA, dihydrorhodamine 123 (DHR123), DAPI, and luminol were from Sigma–Aldrich.

4.3. Sequencing of NCF1 and NCF2

Sequencing was performed for all exons and exon–intron boundaries of *NCF1* and *NCF2* as previously described [24] using ABI310 automated genetic analyzer using *NCF1* and *NCF2* specific primers.

4.4. Isolation of peripheral blood neutrophils

Neutrophils were purified using a standard technique from heparinized peripheral blood using MonoPoly mixture (Flow Laboratories, McLean, VA). The neutrophil-enriched fraction was further purified to >97% by immunomagnetic negative selection (StemCell Technologies). All procedures were carried out under sterile and endotoxin-free conditions.

Subcellular fractionation of neutrophils was carried out according to standard technique previously described. Flotillin was used as a membrane marker.

4.5. Preparation of activated T-cells

Activated T-cells were prepared by incubating peripheral blood mononuclear cells in an OKT3-coated flask in the presence of 350 U/ml IL-2 as previously described [24].

4.6. Measurement of ROS production

Purified neutrophils were loaded with DHR123 at 5 μg/mL for 5 min at 37 °C. Cells were washed, stimulated with PMA (100 ng/ml for 30 min at 37 °C), and ROS production was quantified via flow cytometry (FACSCalibur, Becton Dickinson) by measuring intracellular rhodamine. Alternatively, ROS production was quantified using a standard chemiluminescence method.

4.7. Generation and purification of Hph-1-fusion protein and protein transduction

Hph-1-protein constructs were generated by using the primers shown in Fig. 2B. EGFP, p47^{phox}, and p67^{phox} were amplified from pEGFP-N1 plasmid, NCF-1 cDNA clone (FCC117E05 obtained from TOYOBO), and cDNA from control peripheral lymphocytes, respectively. The amplified fragment and Hph-1 was combined and cloned into pET28b (+) plasmid (Novagen) as previously described. Gal4 construct was described elsewhere.

Protein induction was carried out as previously described [16]. Prepared protein was treated with Detoxi-Gel™ Endotoxin Removing gel (Takara Bio) to eliminate endotoxin.

The cells were incubated with Hph-1 recombinants in PBS at indicated concentrations for indicated time, washed and then were subjected to further analysis.

4.8. Western blotting

Neutrophil lysates were prepared using a lysis buffer (50 mM Tris–HCl, pH 7.5, 150 mM NaCl, 0.25 M sucrose, 5 mM EGTA, 5 mM EDTA, 15 μg/ml leupeptin, 10 μg/ml pepstatin, 10 μg/ml aporotinin, 2.5 mM PMSF, 1.0% NP-40, 0.25% sodium deoxycholate, 10 mM sodium pyrophosphate, 25 mM NaF, 5 mM Na_3VO_4, 25 mM β-glycerophosphate). Western blotting was carried out as described previously [25].

4.9. Immunofluorescence staining

Cytospin preparations of neutrophils were air-dried and fixed for 10 min with paraformaldehyde in PBS, and then permeabilized using acetone at −20 °C for 20 min, washed, and incubated with the indicated antibodies. Nuclei were counterstained with DAPI. The slides were analyzed with a fluorescence microscope (FV10i, Olympus) equipped with Fluoview viewer and review station.

4.10. Statistical analysis

Student's *t*-test was used for statistical analysis.

Acknowledgments

Authors thank Dr. Evan Rachlin for discussion and critical comment. This work was supported in part by grants from the Ministry of Health, Labour, and Welfare of Japan (TM) and from the Ministry of Education, Culture, Sports, Science and Technology of Japan (TM).

References

[1] R.A. Seger, Modern management of chronic granulomatous disease, Br. J. Haematol. 140 (2008) 255–266.
[2] G.M. Bokoch, B. Diebold, J.S. Kim, D. Gianni, Emerging evidence for the importance of phosphorylation in the regulation of NADPH oxidases, Antioxid. Redox Signal. 11 (2009) 2429–2441.
[3] J.A. Winkelstein, M.C. Marino, R.B. Johnston Jr., J. Boyle, J. Curnutte, J.I. Gallin, H.L. Malech, S.M. Holland, H. Ochs, P. Quie, R.H. Buckley, C.B. Foster, S.J. Chanock, H. Dickler, Chronic granulomatous disease. Report on a national registry of 368 patients, Medicine (Baltimore) 79 (2000) 155–169.
[4] B.H. Segal, P. Veys, H. Malech, M.J. Cowan, Chronic granulomatous disease: lessons from a rare disorder, Biol. Blood Marrow Transplant. 17 (2011) S123–S131.
[5] S.R. Schwarze, K.A. Hruska, S.F. Dowdy, Protein transduction: unrestricted delivery into all cells?, Trends Cell Biol. 10 (2000) 290–295.
[6] J.S. Wadia, S.F. Dowdy, Protein transduction technology, Curr. Opin. Biotechnol. 13 (2002) 52–56.
[7] J.M. Gump, S.F. Dowdy, TAT transduction: the molecular mechanism and therapeutic prospects, Trends Mol. Med. 13 (2007) 443–448.
[8] G.P. Dietz, M. Bahr, Delivery of bioactive molecules into the cell: the Trojan horse approach, Mol. Cell. Neurosci. 27 (2004) 85–131.
[9] T. Yoshikawa, T. Sugita, Y. Mukai, Y. Abe, S. Nakagawa, H. Kamada, S. Tsunoda, Y. Tsutsumi, The augmentation of intracellular delivery of peptide therapeutics by artificial protein transduction domains, Biomaterials 30 (2009) 3318–3323.
[10] G.G. Prive, A. Melnick, Specific peptides for the therapeutic targeting of oncogenes, Curr. Opin. Genet. Dev. 16 (2006) 71–77.
[11] S. Racanicchi, C. Maccherani, C. Liberatore, M. Billi, V. Gelmetti, M. Panigada, G. Rizzo, C. Nervi, F. Grignani, Targeting fusion protein/corepressor contact restores differentiation response in leukemia cells, EMBO J. 24 (2005) 1232–1242.
[12] A. Toro, M. Paiva, C. Ackerley, E. Grunebaum, Intracellular delivery of purine nucleoside phosphorylase (PNP) fused to protein transduction domain corrects PNP deficiency in vitro, Cell. Immunol. 240 (2006) 107–115.
[13] A. Toro, E. Grunebaum, TAT-mediated intracellular delivery of purine nucleoside phosphorylase corrects its deficiency in mice, J. Clin. Invest. 116 (2006) 2717–2726.
[14] H.Y. Yoon, S.H. Lee, S.W. Cho, J.E. Lee, C.S. Yoon, J. Park, T.U. Kim, S.Y. Choi, TAT-mediated delivery of human glutamate dehydrogenase into PC12 cells, Neurochem. Int. 41 (2002) 37–42.
[15] E.S. Kim, S.W. Yang, D.K. Hong, W.T. Kim, H.G. Kim, S.K. Lee, Cell-penetrating DNA-binding protein as a safe and efficient naked DNA delivery carrier in vitro and in vivo, Biochem. Biophys. Res. Commun. 392 (2010) 9–15.
[16] J.M. Choi, M.H. Ahn, W.J. Chae, Y.G. Jung, J.C. Park, H.M. Song, Y.E. Kim, J.A. Shin, C.S. Park, J.W. Park, T.K. Park, J.H. Lee, B.F. Seo, K.D. Kim, E.S. Kim, D.H. Lee, S.K.

Lee, Intranasal delivery of the cytoplasmic domain of CTLA-4 using a novel protein transduction domain prevents allergic inflammation, Nat. Med. 12 (2006) 574–579.
[17] J. El-Benna, P.M. Dang, M.A. Gougerot-Pocidalo, Priming of the neutrophil NADPH oxidase activation: role of $p47^{phox}$ phosphorylation and NOX2 mobilization to the plasma membrane, Semin. Immunopathol. 30 (2008) 279–289.
[18] J.D. Lambeth, NOX enzymes and the biology of reactive oxygen, Nat. Rev. Immunol. 4 (2004) 181–189.
[19] A.D. Kennedy, F.R. DeLeo, Neutrophil apoptosis and the resolution of infection, Immunol. Res. 43 (2009) 25–61.
[20] W.M. Nauseef, How human neutrophils kill and degrade microbes: an integrated view, Immunol. Rev. 219 (2007) 88–102.
[21] P.M. Dang, A. Stensballe, T. Boussetta, H. Raad, C. Dewas, Y. Kroviarski, G. Hayem, O.N. Jensen, M.A. Gougerot-Pocidalo, J. El-Benna, A specific $p47^{phox}$-serine phosphorylated by convergent MAPKs mediates neutrophil NADPH oxidase priming at inflammatory sites, J. Clin. Invest. 116 (2006) 2033–2043.
[22] K.D. Martyn, M.J. Kim, M.T. Quinn, M.C. Dinauer, U.G. Knaus, p21-activated kinase (Pak) regulates NADPH oxidase activation in human neutrophils, Blood 106 (2005) 3962–3969.
[23] B. Polack, S. Vergnaud, M.H. Paclet, D. Lamotte, B. Toussaint, F. Morel, Protein delivery by Pseudomonas type III secretion system: ex vivo complementation of p67(phox)-deficient chronic granulomatous disease, Biochem. Biophys. Res. Commun. 275 (2000) 854–858.
[24] N. Takahashi, K. Matsumoto, H. Saito, T. Nanki, N. Miyasaka, T. Kobata, M. Azuma, S.K. Lee, S. Mizutani, T. Morio, Impaired CD4 and CD8 effector function and decreased memory T cell populations in ICOS-deficient patients, J. Immunol. 182 (2009) 5515–5527.
[25] T. Morio, S.H. Hanissian, L.B. Bacharier, H. Teraoka, S. Nonoyama, M. Seki, J. Kondo, H. Nakano, S.K. Lee, R.S. Geha, J. Yata, Ku in the cytoplasm associates with CD40 in human B cells and translocates into the nucleus following incubation with IL-4 and anti-CD40 mAb, Immunity 11 (1999) 339–348.

RESEARCH ARTICLE

Human Mutation

OFFICIAL JOURNAL
HGVS
HUMAN GENOME VARIATION SOCIETY
www.hgvs.org

Functional Characterization and Targeted Correction of ATM Mutations Identified in Japanese Patients with Ataxia-Telangiectasia

Kotoka Nakamura,[1] Liutao Du,[1] Rashmi Tunuguntla,[1] Francesca Fike,[1] Simona Cavalieri,[2] Tomohiro Morio,[3] Shuki Mizutani,[3] Alfredo Brusco,[2] and Richard A. Gatti[1,4]*

[1]*Department of Pathology and Laboratory Medicine, UCLA School of Medicine, Los Angeles, California;* [2]*Department of Genetics, Biology and Biochemistry, University of Torino, Medical Genetics Unit, S. Giovanni Battista Hospital, Torino, Italy;* [3]*Department of Pediatrics and Developmental Biology, Tokyo Medical and Dental University Graduate School of Medicine, Tokyo, Japan;* [4]*Department of Human Genetics, UCLA School of Medicine, Los Angeles, California*

Communicated by Michel Goossens

Received 14 June 2011; accepted revised manuscript 15 September 2011.
Published online 17 October 2011 in Wiley Online Library (www.wiley.com/humanmutation).DOI: 10.1002/humu.21632

ABSTRACT: A recent challenge for investigators studying the progressive neurological disease ataxia-telangiectasia (A-T) is to identify mutations whose effects might be alleviated by mutation-targeted therapies. We studied ATM mutations in eight families of Japanese A-T patients (JPAT) and were able to identify all 16 mutations. The probands were compound heterozygotes in seven families, and one (JPAT2) was homozygous for a frameshift mutation. All mutations—four frameshift, two nonsense, four large genomic deletions, and six affecting splicing—were novel except for c.748C>T found in family JPAT6 and c.2639-384A>G found in family JPAT11/12. Using an established lymphoblastoid cell line (LCL) of patient JPAT11, ATM protein was restored to levels approaching wild type by exposure to an antisense morpholino oligonucleotide designed to correct a pseudoexon splicing mutation. In addition, in an LCL from patient JPAT8/9, a heterozygous carrier of a nonsense mutation, ATM levels could also be partially restored by exposure to readthrough compounds (RTCs): an aminoglycoside, G418, and a novel small molecule identified in our laboratory, RTC13. Taken together, our results suggest that screening and functional characterization of the various sorts of mutations affecting the *ATM* gene can lead to better identification of A-T patients who are most likely to benefit from rapidly developing mutation-targeted therapeutic technologies.
Hum Mutat 33:198–208, 2012. © 2011 Wiley Periodicals, Inc.

KEY WORDS: ataxia-telangiectasia; ATM; large genomic deletions; functional analysis of DNA variants; mutation-targeted therapy; Japanese ATM mutation

Introduction

Ataxia-telangiectasia (A-T; MIM# 208900) is an autosomal recessive neurodegenerative disorder characterized by progressive cerebellar degeneration, ocular apraxia and telangiectasia, increased cancer risk, immunodeficiency, sensitivity to ionizing radiation (IR), chromosomal instability, and cell cycle abnormalities [Boder and Sedgwick, 1958; Gatti, 2001]. A-T is caused by mutations in the *ATM* gene (MIM# 607585) that usually encodes a 13 kb transcript that produces a 370 kDa protein [Gatti et al., 1988; Lange et al., 1995; Savitsky et al., 1995]. Intranuclear ATM protein is low or absent in most A-T patients, despite the presence of relatively normal levels of *ATM* transcripts. ATM is activated by autophosphorylation after binding with the MRN (Mre11-Rad50-Nbs) complex at sites of DNA double strand breaks [Bakkenist and Kastan, 2003; Kozlov et al., 2006], and subsequently phosphorylates hundreds of downstream target proteins involved in cell cycle checkpoints, DNA repair, and apoptosis [Bolderson et al., 2009; Matsuoka et al., 2007; Shiloh 2006]. ATM also appears to play a critical role in resolving chronic inflammation [Westbrook and Schiestl, 2010].

A-T patients are usually compound heterozygotes, carrying two distinct mutations. Mutations occur throughout the entire gene without hot spots. Founder effects are commonly observed in many ethnic isolates [Birrell et al., 2005; Campbell et al., 2003; Cavalieri et al., 2006; Gilad et al., 1996a; Laake et al., 1998; McConville et al., 1996; Mitui et al., 2003, 2005; Telatar et al., 1998a, b] wherein patients often carry mutations in a homozygous state. We have previously shown [Du et al., 2007, 2009, 2011; Lai et al., 2004] that accurately analyzing the functional consequences of mutations in individual A-T patients enables the grouping of patients into "mutation categories" that are most likely to be corrected by future customized mutation-targeted therapies.

The aims of the present study were to: (1) characterize the *ATM* mutations in Japanese A-T (JPAT) families; and (2) identify which JPAT patients might be candidates for personalized mutation-targeted therapy. We report that three of eight JPAT families examined are potential candidates for mutation-targeted therapy based on partial restoration of functional ATM protein production.

Materials and Methods

Cell Lines

Lymphoblastoid cell lines (LCLs) [Svedmyr et al., 1975] or activated T-cells [Minegishi et al., 2006] were established from affected

Additional Supporting Information may be found in the online version of this article.

*Correspondence to: Richard A. Gatti, Department of Pathology and Laboratory Medicine, UCLA School of Medicine, 675 Charles E. Young Drive South, Los Angeles, CA 90095-1732. E-mail: rgatti@mednet.ucla.edu

Contract grant sponsors: National Institutes of Health (1R01NS052528); A-T Ease Foundation; A-T Medical Research Foundation.

members of eight Japanese A-T families, including three sibling pairs (JPAT4/5, 8/9, and 11/12). The families came from different geographical regions. Clinical descriptions of patients from these families have been reported previously [Morio et al., 2009].

Short Tandem Repeat (STR) Haplotype Analysis

Standardized STR (short tandem repeat/microsatellite) genotyping for the *ATM* gene region was performed as previously described [Mitui et al., 2003]. Briefly, we used four fluorescently labeled microsatellite markers located within a 1.4 cM region of chromosome 11q22-q23: D11S1819, NS22, D11S2179, and D11S1818. Markers NS22 and D11S2179 are located within the *ATM* gene, in introns 45 and 62, respectively [Udar et al., 1999; Vanagaite et al., 1995]. Allelic sizes were detected with an ABI 3730 DNA analyzer (Applied Biosystems Inc, Carlsbad, CA) and standardized to a reference sample (CEPH 1347-02).

Identification of Mutations

Total RNA was isolated from patient-derived T-cell lines using RNeasy (QIAGEN, Valencia, CA), and cDNA was synthesized using random primers and the Superscript III reverse transcriptase (Invitrogen, Carlsbad, CA). The entire *ATM* coding region was divided into eight overlapping fragments (Regions 1–8) ranging from 1,500 to 1,800 bps [Du et al., 2008]. These regions were PCR amplified and then sequenced using 19 different primers. Mutations on the cDNA level were confirmed in genomic DNA (gDNA) by sequencing relevant exon and intron boundaries. Mutation analysis is based on the same ATM reference sequence used for ATM mutations in the Leiden Open Variation Database (www.LOVD.nl/ATM; NCBI reference sequence:NM_000051.3).

Maximum Entropy Scores and Search for Exonic Splicing Enhancers (ESEs)

The strength of the 5′ and 3′ splice sites (ss) was determined by calculating and comparing the wild-type and mutant 5′ and 3′ ss using the Maximum Entropy software available at http://genes.mit.edu/burgelab/maxent/Xmaxentscan_scoreseq.html [Eng et al., 2004; Mitui et al., 2009; Yeo and Burge, 2004]. We scanned for putative binding motifs for serine/arginine-rich (SR) proteins using the ESEfinder software available at http://rulai.cshl.edu/tools/ESE [Cartegni et al., 2003; Smith et al., 2006].

Long-Range PCR and Breakpoint Regions for Genomic Deletions

To amplify large gDNA fragments, 500 ng of gDNA was used as template, followed by 35 cycles of 95C for 1 min, 68°C for 10 min, and extension at 72°C for 15 min using EX Taq polymerase according to the manufacturer's protocol (Takara Bio Inc, Shiga, Japan). Fragments containing large genomic deletions (LGDs) were isolated from agarose gels and sequenced to determine the breakpoints.

Multiplex Ligation-dependent Probe Amplification (MLPA)

A total of 100 ng of gDNA was used as starting material for the SALSA MLPA P041 and P042 *ATM* kits (MRC-Holland, Amsterdam, Netherlands, www.mrc-holland.com) [Schouten et al., 2002]. The P041 probe mix contained probes for 33 of the 65 exons as well as three probes for exon 1. The P042 *ATM* probe mix contained probes for the remaining *ATM* exons. Both probe mixtures also contained probes for control genes. After hybridization, ligation, and amplification, according to the instructions of the manufacturer, 1 μl of PCR product was mixed with 0.2 μl of ROX-500 labeled internal size standard, separated on an ABI Prism 3100 Avant automatic sequencer (Applera, Norwalk, Connecticut, CA), and analyzed using the GeneScan software ver.3.1. For MLPA data analysis, we used Coffalyser MLPA DAT software developed by MRC-Holland. For each probe, a range from 1 ± 0.2 was considered as a normal exon dosage, while a deletion was determined as being between 0.3 and 0.7.

Antisense Morpholino Oligonucleotide (AMO) Design and Treatment

A 25-mer antisense morpholino oligonucleotide (AMO) was designed to target the 5′ aberrant splice site of a pseudoexon mutation in pre-mRNA of JPAT11/12. The AMO-J11 sequence was: CCTGGAAAAATACTTACAATTAAAC. AMO748C (ATTCACACACTCGAATTCGAAAGTT) and AMO4956GC (CTTGGATAACTGCAACAAATTGACA) were designed to target wild-type sequences to determine potential regulatory elements at the site of a mutation(s). AMOs were synthesized by Gene-Tools (Philomath, OR). Treatment of LCLs with AMOs was performed as previously described [Du et al., 2007]. Cells were suspended in 5% FBS/RPMI medium and the AMO was added directly to medium at the concentrations indicated. Endo-Porter (Gene-Tools) was added to the medium to assist in intracellular incorporation of the AMO. Cells were collected after 48 hr for RNA analysis, and after 84 hr for ATM protein detection. Vivo-AMO was also used to treat JPAT 11 to enhance cellular delivery (Gene-Tools).

Irradiation Induced ATM-Ser1981 Foci Formation (IRIF)

Immunostaining of nuclear foci of ATM-Ser1981was performed as described [Du et al., 2007, 2009]. In brief, LCLs were first treated with the relevant compounds for 4 days before being irradiated with 2 Gy and then incubated at 37°C for 30 min. Next, the cells were fixed with 4% paraformaldehyde and then permeabilized on cover slips. The cover slips were blocked for 1 hr and incubated with mouse anti-ATM pSer1981 for 1 hr (1:500; Cell Signaling Technology, Danvers, MA). After a second blocking, cells were stained with Alexa Fluor 488 anti-mouse IgG (1:150; Invitrogen) for 1 hr and mounted onto slides.

Flow Cytometry Analysis of ATM-Ser1981 Autophosphorylation (FC-ATM-pSer1981)

FC-ATM-pSer1981 was used to verify the restoration of Ser1981 autophosphorylation by readthrough compounds (RTCs) [Du et al., 2009; Nahas et al., 2009]. The cells were treated for 4 days with RTCs, resuspended in PBS, and irradiated with 10 Gy. After 1 hr, the cells were fixed and permeabilized using FIX & PERM (Invitrogen). The cells were then incubated with 1 μl of mouse ATM-s1981 antibody (Cell Signaling Technology) for 2 hr at room temperature. After this time, cells were washed and resuspended in 100-μl PBS with Alexa Fluor 488 anti-mouse IgG (Invitrogen) for 45 min, and then washed and resuspended in PBS with 0.2% paraformaldehyde, before being analyzed using a FACSCalibur (BD, Franklin Lakes, NJ).

Western Blotting

Nuclear extracts were prepared by following the NE-PER protocol (Thermo Fisher Scientific, Rockford, IL). Proteins were separated

on a 7.5% SDS-polyacrylamide gel. Western blots were prepared as described [Du et al., 2007], and probed with anti-ATM (Novus Biologicals, Littleton, CO), -SMC1, or -KAP1 antibodies (Novus Biologicals).

Results

Mutation Analysis

We initially screened our A-T patients for two previously reported Japanese mutations, c.4776(IVS33)+2T>A and c.7883_7887delTTATA [Ejima and Sasaki 1998; Fukao et al., 1998]. Neither of these mutations was detected.

STR genotyping of the *ATM* genomic region was performed for 11 JPAT patients, but since parental gDNAs were unavailable, we could only verify that one patient was homozygous for all markers (JPAT2): [S1819, 131; NS22, 165; S2179, 143; S1818, 162] [Mitui et al., 2003]. As a result, we set out to directly sequence the entire *ATM* coding region after PCR amplifying eight partially overlapping fragments from patients' cDNA [Du et al., 2008]. We identified 12 of the 16 expected mutations (75%) and confirmed them upon sequencing gDNA (Table 1). Only one patient (JPAT2) was homozygous, suggesting that most JPAT patients do not result from consanguineous marriages. The 12 mutations included four frameshifts (counting the homozygous JPAT2 twice), two nonsense, and six splice variants (Table 1). The remaining mutations (4/16; 25%) were four LGDs, which we identified after performing long-range PCR using gDNA as template. Fourteen mutations were novel; two had been previously reported: c.748C>T in JPAT6 [Teraoka et al., 1999] and c.2639-384A>G in JPAT11/12 [Sobeck 2001]. All mutations resulted in the absence of ATM protein (Supp. Fig. S1 and data not shown).

Splicing Mutations

The six splicing mutations identified were analyzed by using Maximum Entropy software (MaxENT) to estimate the strength of the splice sites [Yeo and Burge, 2004] and type of splice defect [Eng et al., 2004]. The mutations found are described below, and diagrams for potential splicing mechanisms are shown in Figure 1.

(1) c.331+5G>A (IVS6): This mutation changed the MaxENT score of the 5′ ss from 9.8 to 3.6. A shorter PCR product compatible with exon 6 skipping was observed at the cDNA level in patient JPAT1 using primers for exons 4 and 7 (Figs. 1 and 2A, lane 3).

(2) c.748C>T: cDNA from patient JPAT6 showed skipping of exon 9 (Figs. 1and 2B, lane 5). This allele with substitution c.748C>T predicted an amino acid change from Arg to a stop codon (CGA >TGA). Given that c.748C>T did not affect the scores for consensus splice sites, nor affect an ESE site, we hypothesized that it affected an as yet unknown splicing regulatory element. To test this idea further, we designed an AMO targeting the wild-type sequence at the site of the mutation in order to block the interaction between any regulatory molecule(s) and the wild-type sequence. Wild-type cells treated with increasing concentrations of AMO748C (Fig. 2G) showed skipping of exon 9, supporting idea model that the region around nucleotide 748 most likely contains a regulatory splicing motif.

(3) c.2639-384A>G (IVS19): The c.2639-384A>G variant in patient JPAT11/12 creates a novel splice acceptor site within IVS19 (Fig. 1), thereby creating a cryptic splice and "pseudo-exon" of 58 bp is created in intron 19 (Fig. 2C, lanes 5 and 6).

Table 1. Mutations of Eight Japanese Families

Ex/Int	Patient	cDNA change	Genomic DNA mutation	Consequence
IVS6	JPAT1[a]	c.186_331del146 (deletes exon 6)	**c.331+5G>A (5′ss 9.81>3.58)**	Aberrant splicing (IV)
7	JPAT6[a]	c.397_398insT	**c.397_398insT**	Frameshift
9	JPAT6[b]	c.663_901del239 (deletes exon 9)	c.748C>T (R>X)	Aberrant splicing (III)
10	JPAT8/9[a]	c.902_1065del164 (deletes exon 10)	**c.902-19_1065+869del1052**	Large genomic deletion
IVS19	JPAT11/12[a]	c.2639_2640ins58	c.2639-384A>G (5′ss 0.36>8.54)	Aberrant splicing (II)
IVS19	JPAT3[a]	c.2639_2838del200 (deletes exon 20)	**c.2639-19_2639-7del13 (3′ss 8.8>3.4)**	Aberrant splicing (IV)
20	JPAT8/9[b]	c.2877C>G	**c.2877C>G (Y>X)**	Nonsense (TAG)
35	JPAT4/5[a]	c.4910_5005del96 (deletes exon 35)	**c.4956GC>TT (1Q>FX)**	Aberrant splicing (III)
38	JPAT1[b]	c.5415G>A	**c.5415G>A (W>X)**	Nonsense (TGA)
IVS48	JPAT11/12[b]	c.6808_7515del708 (deletes ex 49-52)	**c.6807+272_7516-275del5350**	Large genomic deletion
55	JPAT4/5[b]	c.7925_7926del2(GA)	**c.7925delGA**	Frameshift
60	JPAT10[a]	c.8419_8584del166 (deletes exon 60)	**c.8419-643_8507del732**	Large genomic deletion
61	JPAT10[b]	c.8585_8671del87 (deletes exon 61)	**c.8585-1G>C (5′ss 10.2>2.0)**	Aberrant splicing (IV)
61	JPAT2[h]	c.8624delA	**c.8624delA**	Frameshift
IVS63	JPAT3[b]	c.8851_9697del847	**c.8852-2kbdel17kb (CRAT [B] mutation?)**	Large genomic deletion

Bolded mutations have not been reported previously.
[a]First allele.
[b]Second allele.
[h]Homozygote.
Nucleotide numbering is based on +1 being the A of the first translation start codon in exon 4 (NCBI reference sequence: NM_000051.3).

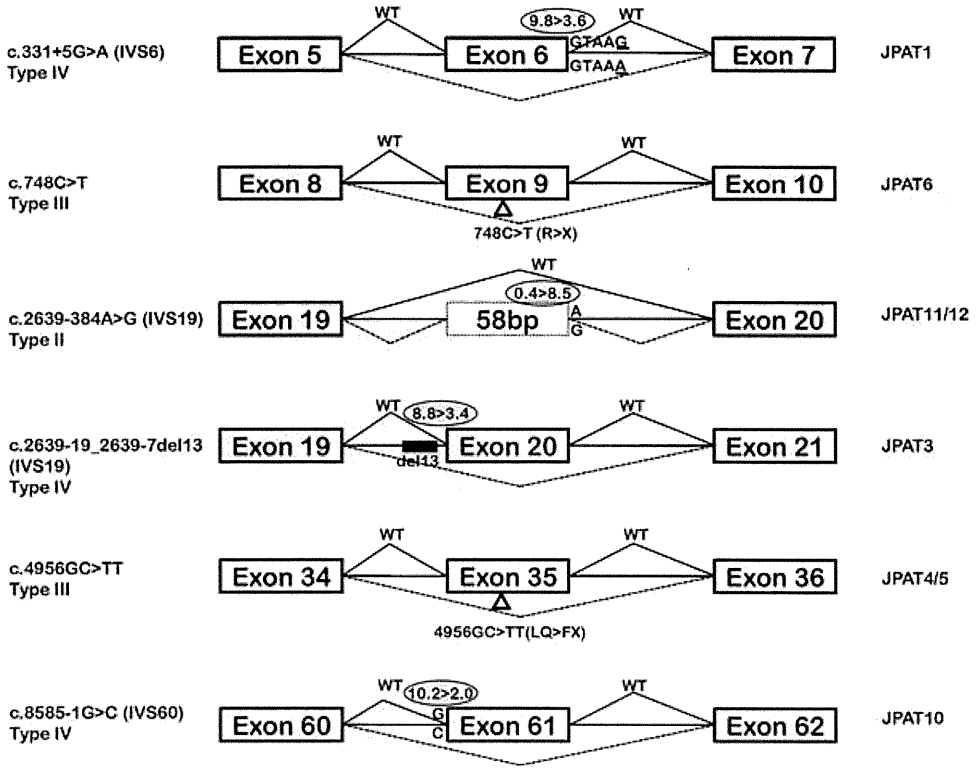

Figure 1. *ATM* splicing mutations. Genomic mutations causing splicing mutations were analyzed for changes in splicing scores calculated by Max ENT. Classification of splicing mutations is reported accordingly to Eng et al. [2004]. See text for additional details.

This results in a frameshift and a predicted secondary premature stop codon.

(4) c.2639-19_2639-7del13 (IVS19): In Figure 2D (lane 3), the PCR products from JPAT3 cDNA showed a normal and an additional prominent lower band (783 bp and 583 bp, respectively). Sequencing of the 583-bp band revealed skipping of exon 20. gDNA sequencing identified a 13 nt deletion in intron 19 at position c.2639-19_2639-7. The 3′ MaxENT score changed from 8.8 to 3.4 (Fig. 1).

(5) c.4956GC>TT: In family JPAT4/5, we identified a c.4956GC>TT substitution within exon 35 (p.LQ1652_1653FX) that leads to skipping of exon 35 without affecting an ESE or canonical splice sites (Figs. 1 and 2E, lanes 3 and 4). Exposing wild-type LCLs to increasing concentrations of AMO4956GC, targeting the mutation site, revealed skipping of exon 35 (Fig. 2H); these results suggest that nucleotide 4956 is part of a regulatory protein binding site, which when disrupted influences the aberrant splicing observed in JPAT4/5.

(6) c.8585-1G>C (IVS60): JPAT10 harbors the IVS60-1G>C mutation that changed the MaxENT score of the 3′ ss from 10.2 to 2.0, resulting in a skipping of the exon 61 (Fig. 2F, lane 4). Interestingly, the second allele of this patient was a splicing mutation that is predicted to result in exon 60 skipping (Fig. 2F, lane 4). We sequenced gDNA for exons 59–62 but failed to find a mutation that would account for the skipping of exon 60 (however, see additional results on JPAT10 below).

Large Genomic Deletions (LGDs)

(1) c.902-19_1065+869del1052 (del ex10): Two siblings (JPAT8/9) yielded an abnormal 369-bp fragment when cDNA was amplified from exon 9 to 11 (Fig. 3A, cDNA gel, lanes 3 and 4). When this band was isolated and sequenced, we found a deletion of exon 10. No mutation was observed in exons 9–11, ruling out a conventional splicing mutation. Using long-range PCR to amplify the genomic region from exon 9 to 11, we obtained a 3.3 kb fragment (Fig. 3A, gDNA gel lanes 3 and 4), whose sequence revealed a 1,052-bp deletion from IVS9-19 to IVS10+869; this deletion included exon 10 (164 bp).

(2) c.6807+272_7516-275del5350 (del ex49-52): Two siblings (JPAT11/12) showed an abnormal PCR fragment of 1.1 kb when cDNA was amplified from exon 48 to 53 (Fig. 3B, cDNA gel). The sequence of the PCR product showed a deletion of exons 49–52. A long-range PCR performed on gDNA using primers for exons 48 and 53 produced a 1.1 kb band instead of the expected 6.4 kb (Fig. 3B, left). Sequencing of the 1.1 kb band revealed a 5,350-bp genomic deletion that starts in intron 48 and ends in intron 52.

(3) c.8419-643_8507del732 (del ex 60): In patient JPAT10, we suspected that skipping of exon 60 might reflect an LGD. We amplified the gDNA surrounding exons 59–61 and found a 732-bp genomic deletion extending from IVS59-643 to nucleotide 89 of exon 60 (Fig. 3C).

(4) c.8851-2kbdel17kb (del ex64-65): When mutation screening failed to identify a second pathogenic mutation in JPAT3, we were prompted to search for an LGD mutation with Multiplex Ligation-dependent Probe Amplification (MLPA). We observed a significant decrease in peak height for the final exons 64 and 65, indicative of a deletion carried in heterozygous state (Fig. 4A). Previous studies have demonstrated two LINE-1 sequences between IVS63 and downstream of exon 65, as well as a 17 kb genomic deletion in the *ATM* gene of A-T patients

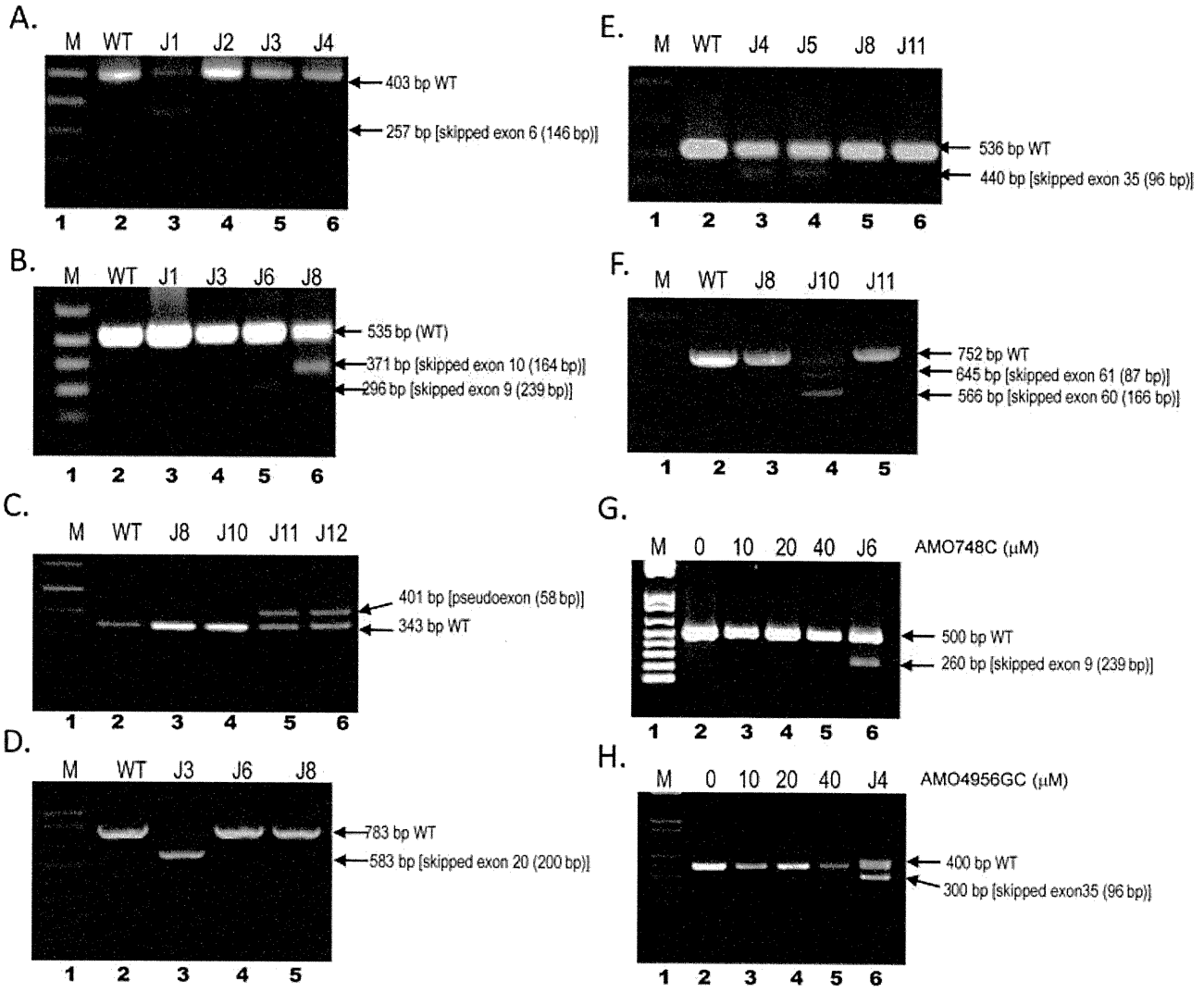

Figure 2. Effect of splicing mutations on cDNA. Agarose gel images of PCR products showed aberrant spliced products. Patient cDNA were used as templates for PCR amplifications in the regions displaying splicing mutations. M (lane 1) is 1 kb plus ladder (Invitrogen), wild-type cDNA was used as control (lane 2). **(A)** Skipped exon 6 in JPAT1 (lane 3). **(B)** Skipped exon 9 in JPAT6 (lane 5) and skipped exon 10 in JPAT8 (lane 6). **(C)** Pseudoexon of JPAT11 and JPAT12 (lanes 5 and 6). **(D)** Skipped exon 20 in JPAT3 (lane 3). **(E)** Skipped exon 35 in JPAT4 and JPAT5 (lanes 3 and 4). **(F)** Skipped exons 60 and 61 in JPAT10 (lane 4). **(G)** AMO-treated wild-type lymphoblastoid cell line (LCL) produced alternative spliced product that skipped exon 9. JPAT6, carrying the c.748C>T mutation, showed a skipped exon 9 product (lane 6), **(H)** AMO 4956GC treated wild-type LCL produced alternative spliced product that skipped exon 35. JPAT4 that has 4956GC>TT mutation showing skipped exon 35 products as a control (lane 6). See text for additional details.

with Costa Rican, Dutch, and Brazilian backgrounds [Broeks et al., 1998; Coutinho et al., 2004; Mitui et al., 2003; Telatar et al., 1998b].

Figure 4B summarizes the locations of primers, LINE-1 sequences, and an LGD for this region.

We used two sets of primers: Primer set #1 (P1Fw and P4Rev) was 23 kb apart, flanking the 17 kb deletion. Because of the nature of our PCR conditions, no PCR product was anticipated from the wild-type allele, while the mutant allele should yield a 6 kb fragment. Primer set #2 (P2Fw and P3Rev) was placed within the 17 kb deletion, which should have produced a 2.4 kb fragment from only the wild-type allele [Telatar et al., 1998b]. Figure 4B (lane 2) shows that wild-type gDNA produced the 2.4 kb fragment, while CRAT [B] (a Costa Rican patient homozygous for a 17 kb deletion) produced the 6 kb fragment (lane 4). A CRAT [B] heterozygote produced both the 2.4 kb fragment and the 6 kb product from the deletion (Fig. 4B, lane 5). The CRAT [B] band pattern was also observed in the gDNA of JPAT3, suggesting the presence of an LGD between two LINE-1 sequences (Fig. 4B, lane 3). Available breakpoints and surrounding sequences were analyzed using Repeat Masker software to search for flanking repetitive elements [Babushok and Kazazian, 2007; Kazazian and Goodier, 2002; Telatar et al., 1998b] (see Fig. 3). Because the breakpoint was in a highly homologous repeat sequence, the ends could not be accurately determined. The other Japanese patient (JPAT8) who did not have a deletion in this region showed a pattern identical to the wild type (Fig. 4B, lane 6).

The STR haplotypes for JPAT3, CRAT [B], and BRAT3 differed. JPAT3: S1819 [131,133]; NS22 [173,175]; S2179 [137,137]; S1818 [160,168]; CRAT [B]: S1819 [131]; NS22 [171]; S2179 [141]; S1818 [160] [Mitui et al., 2003]; BRAT 3: S1819 [133]; NS22 [155]; S2179

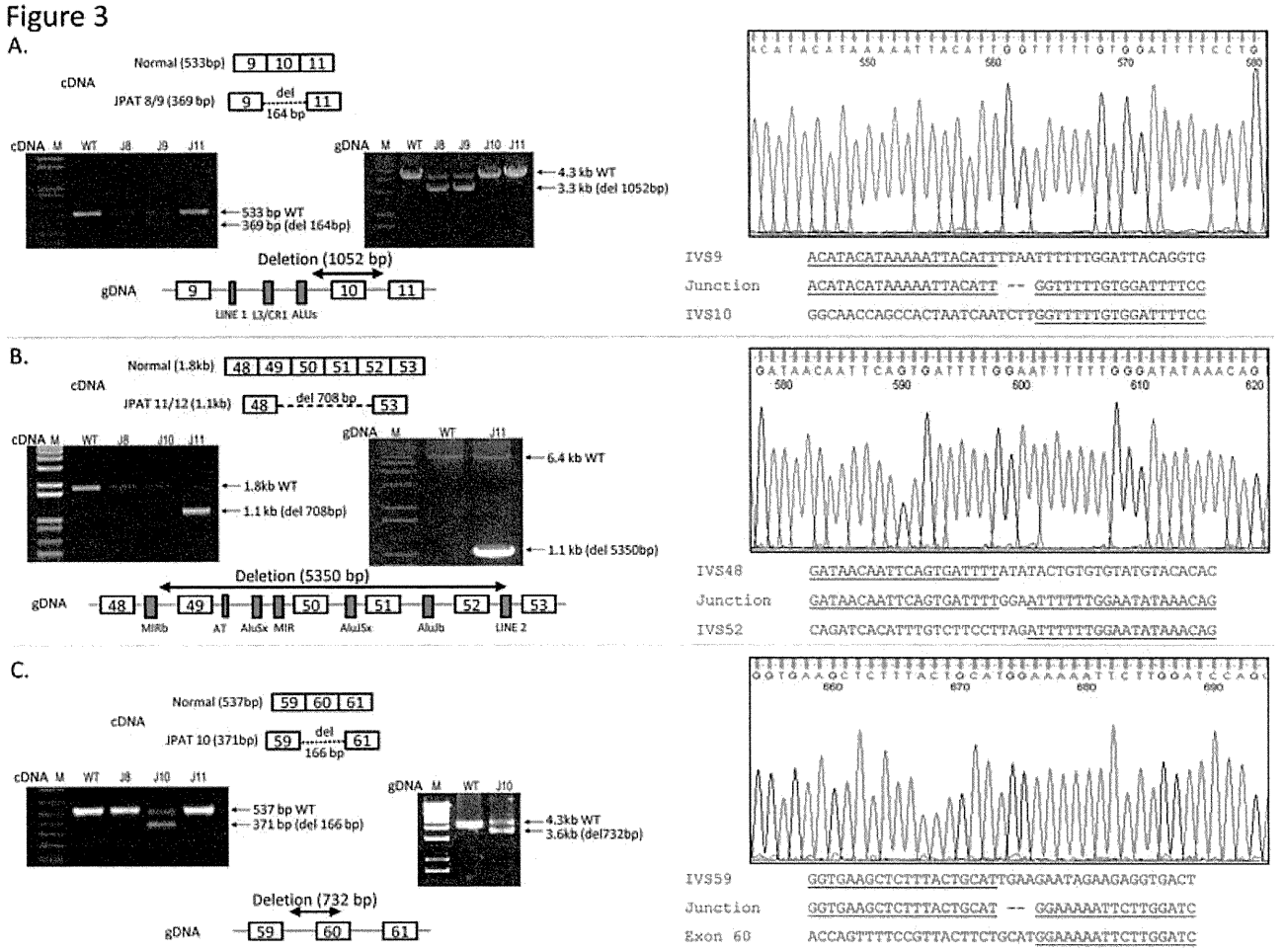

Figure 3. Large genomic deletions (LGDs). **(A)** Schematic representation of cDNA showing deletion of exon 10 and agarose gel image of PCR products (using primers GFw and GRev) (left): Lane 1 is 1 kb plus ladder (Invitrogen), lane 2 is wild-type control, lane 3 (JPAT8) and lane 4 (JPAT9) showing deletion of exon 10, lane 5 is JPAT control. Agarose gel image (right) for genomic DNA (gDNA) PCR products (using primers EX9Fw and EX11Rev) showing deletion of 1 kb in JPAT8/9. Schematic representation of DNA shows LGD, as well as repetitive elements within the region (at bottom). Sequence data with junction sequences are shown on right. **(B)** Schematic representation of cDNA change in JPAT11/12 between exon 48 and exon 53, which are analyzed by PCR (using primers FATFw and FATRev). Agarose gel image (left) for cDNA shows aberrant spliced products of JPAT11 (lane 5). Lane 1 is 1 kb plus ladder, lane 2 is wild-type, lanes 3 and 4 are JPAT control. Agarose gel image (right) for gDNA shows deletion of 5.3 kb (using EX Taq polymerase with LREX48Fw and LREX53Rev primers). Schematic representation of gDNA (at bottom) shows large deletion. Sequence data with junction sequences are shown on right. **(C)** Schematic representation of JPAT10 cDNA shows deletion of exon 60. Agarose gel image (left) shows aberrant spliced products. Agarose gel image (right) for gDNA PCR products (using primers EX59Fw and EX61Rev) show reduced size in JPAT10 (3.6 kb) compared to wild type (4.3 kb) and schematic representation of gDNA showing deletion at c.8269-643del732, which includes the first 89 bp of exon 60. Sequences are shown at right.

[147]; S1818 [146] [Mitui et al., 2003]. These results suggested that the c.8851-2kbdel17kb mutations in the three patients were not ancestrally related.

Correction of Type II Pseudoexon Splicing Mutation using an AMO

In family JPAT11/12, we identified a type II splicing mutation [Eng et al., 2004] c.2639-384A>G, which created a cryptic acceptor splice site resulting in the inclusion of 58 bp of intronic sequence (Figs. 2C and 5A). We designed AMO-J11 to target the cryptic 5′ splice site (Fig. 5A) [Du et al., 2007; Eng et al., 2004]. The LCL of JPAT11 was treated with AMO-J11 for 4 days followed by RT-PCR analysis. Mutant splicing was almost completely abrogated in an AMO dose-dependent manner and normal transcript was restored (Fig. 5B). Nuclear extracts from treated JPAT11 cells also showed a full-length ATM protein (data not shown). In order to enhance the delivery and efficiency of the AMO, we also designed a structurally modified AMO referred as "Vivo-AMO" [Morcos et al., 2008; Moulton and Jiang, 2009]. Notably, a significant amount of functional ATM protein was induced by 0.5 μM Vivo AMO-J11 (Fig. 5C). However, "Vivo-AMO" started to show possible cytotoxicity at 0.8μM (Fig. 5C, lane 4).

Correction of Nonsense Mutation in JPAT8 using RTCs

The JPAT8/9 siblings lack ATM protein because they carry an LGD and a nonsense mutation (c.2877C>G, p.Tyr959X). Functional ATM protein is inducible with compounds that readthrough premature termination codons [Du et al., 2009] even when the LCL carries the nonsense mutation in a heterozygous state [Lai et al., 2004]. We treated JPAT8 LCL with the readthrough compound RTC13 for 4

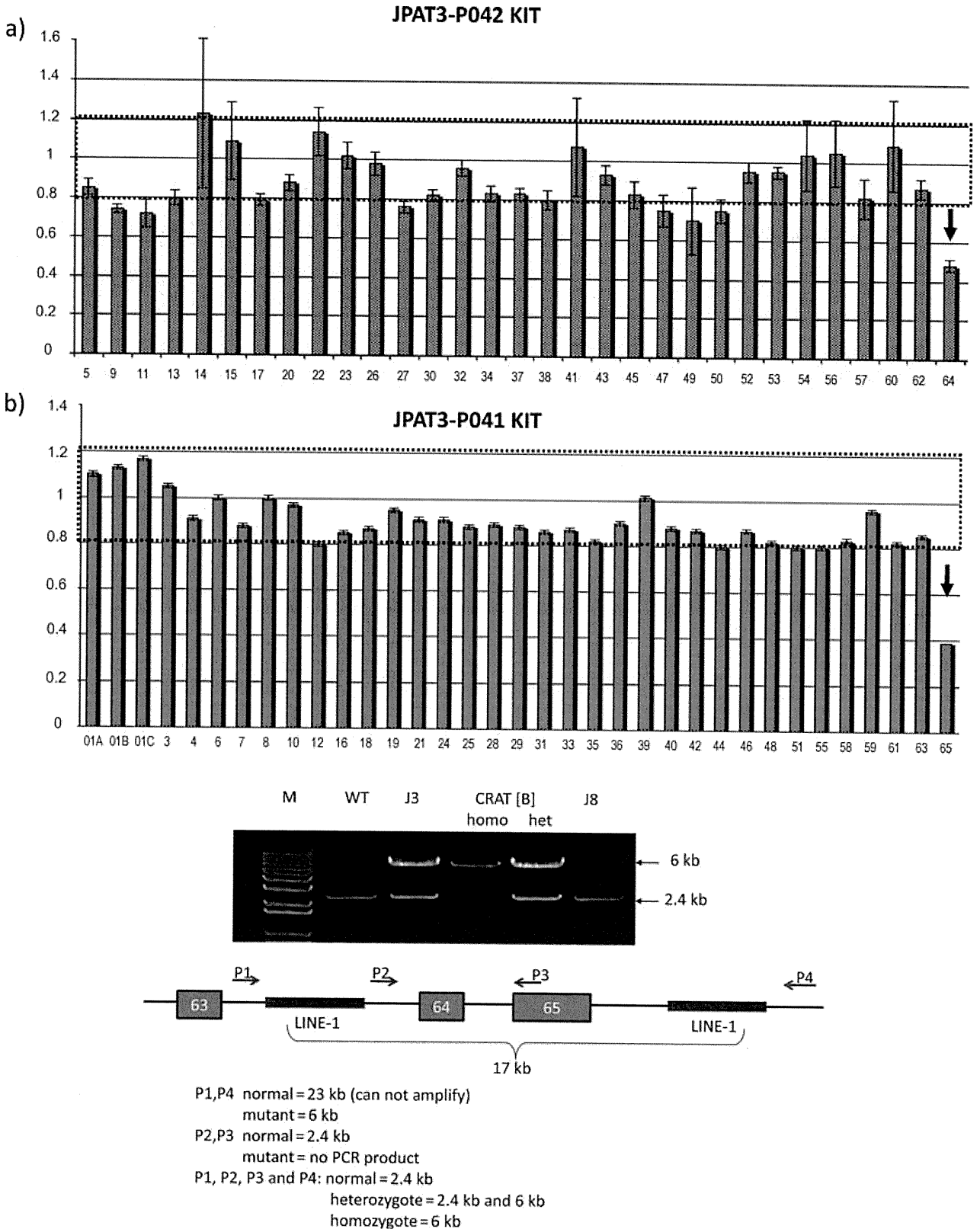

Figure 4. Analysis of LGD in patient JPAT3. **(A)** Multiplex Ligation Probe Amplification (MLPA) analysis using MLPA P041 **(A)** and P042 **(B)** kits. For each of the two analyses normalized peak area histograms of JPAT3 are shown. The dotted lines indicate the normal exon dosages between 0.8 and 1.2. The heavy black arrows indicate the exon probes of decreased signal, corresponding to the genomic deletion of exons 64 and 65. **(B)** PCR products depicting a LGD between two LINE-1 sequences. Lane 1 is 1 kb plus ladder, lane 2 is wild-type control, lane 3 is JPAT3, lane 4 is homozygous CRAT [B] patient with a very similar mutation, lane 5 is a heterozygous individual with CRAT [B] mutation, lane 6 is JPAT8. Schematic diagram (below) shows the relative locations for four different primers at the region of the LGD.